Mantle source and melting processes beneath Iceland's Flank and Rift Zones: Forward Modelling of Heterogeneous Mantle Melting

Emma Christina Waters[1], Oliver Shorttle[2], Sæmundur Ari Halldórsson[3], Katsura Kobayashi[4], David Neave[5], Ray Burgess[5], and Margaret E Hartley[5]

[1]University of Glasgow
[2]University of Cambridge
[3]University of Iceland
[4]ISEI, Okayama University
[5]University of Manchester

January 3, 2023

Abstract

The Icelandic mantle contains a range of lithologies associated with the depleted upper mantle, a mantle plume, and recycled oceanic lithosphere but the precise nature of depleted and enriched components in the mantle and their relative contributions to melt production remain poorly constrained. In this study, we collect new olivine- and plagioclase-hosted melt inclusion data and compile this with existing literature data to investigate the relative contributions from different mantle lithologies to basaltic magmas erupted in Icelandic flank zones and neovolcanic zones by modelling the melting of a heterogeneous mantle and subsequent mixing of derived melts. We find that observed melt inclusion compositions from off-axis flank zones are best explained as homogenized mixtures of pyroxenite- and lherzolite-derived melts produced at depths around 80-93 km, by which point lherzolite has only experienced a low degree of melting whereas the pyroxenite lithology has melted extensively. These melts represent the onset of channelization in the mantle and are transported rapidly to the surface without input from shallower melts. Melt compositions from the on-axis neovolcanic zones and off-axis Öræfajökull, are produced by mixing this deep melt component with higher degree lherzolite melts produced at shallower depths, between 57-93 km. Proportions of shallow lherzolite-derived melts and deep homogenized melt vary, but the lowest contribution from the deep homogenized melt is seen in the Northern Volcanic Zone. Ourresults support a model whereby deep melts mix until melt channelization starts in the mantle, after which binary mixing between the homogenized deep melt and shallower fractional melts occurs.

Hosted file

951818_0_art_file_10522623_rmmy9z.docx available at https://authorea.com/users/565277/articles/612265-mantle-source-and-melting-processes-beneath-iceland-s-flank-and-rift-zones-forward-modelling-of-heterogeneous-mantle-melting

Hosted file

951818_0_supp_10522670_rmmtl6.docx available at https://authorea.com/users/565277/articles/612265-mantle-source-and-melting-processes-beneath-iceland-s-flank-and-rift-zones-forward-modelling-of-heterogeneous-mantle-melting

Mantle source and melting processes beneath Iceland's Flank and Rift Zones: Forward Modelling of Heterogeneous Mantle Melting

E. C. Waters[1,2]*, O. Shorttle[3], S. A. Halldórsson[4], K. Kobayashi[5], D. A. Neave[1], R. Burgess[1], M. E. Hartley[1]

[1] Department of Earth and Environmental Sciences, University of Manchester, Manchester, M13 9PL, UK.

[2]School of Geographical and Earth Sciences, University of Glasgow, Glasgow, G12 8QQ, UK.

[3]Department of Earth Sciences, University of Cambridge, Cambridge, CB2 3EQ, UK.

[4]Nordic Volcanological Center, Institute of Earth Sciences, University of Iceland, Reykjavík, Iceland

[5]The Pheasant Memorial Laboratory for Geochemistry and Cosmochemistry, Institute for the Study of the Earth's Interior, Okayama University, Misasa, 682-0193, Japan

Corresponding author: Emma Waters (emma.waters@glasgow.ac.uk)

Key Points:

- SFZ and Surtsey melts are a homogenized mixture of enriched pyroxenite-derived melts and low-degree lherzolite-derived melts
- Deep homogenized melts mix with shallower lherzolite-derived melts to produce melt compositions of Icelandic neovolcanic zones
- A pyroxenite lithology is required for melt generation in Iceland's neovolcanic zones, with the lowest contribution observed in the NVZ

Abstract

The Icelandic mantle contains a range of lithologies associated with the depleted upper mantle, a mantle plume, and recycled oceanic lithosphere but the precise nature of depleted and enriched components in the mantle and their relative contributions to melt production remain poorly constrained. In this study, we collect new olivine- and plagioclase-hosted melt inclusion data and compile this with existing literature data to investigate the relative contributions from different mantle lithologies to basaltic magmas erupted in Icelandic flank zones and neovolcanic zones by modelling the melting of a heterogeneous mantle and subsequent mixing of derived melts. We find that observed melt inclusion compositions from off-axis flank zones are best explained as homogenized mixtures of pyroxenite- and lherzolite-derived melts produced at depths around 80-93 km, by which point lherzolite has only experienced a low degree of melting whereas the pyroxenite lithology has melted extensively. These melts represent the onset of channelization in the mantle and are transported rapidly to the surface without input from shallower melts. Melt compositions from the on-axis neovolcanic zones and off-axis Öræfajökull, are produced by mixing this deep melt component with higher degree lherzolite melts produced at shallower depths, between 57-93 km. Proportions of shallow lherzolite-derived melts and deep homogenized melt vary, but the lowest contribution from the deep homogenized melt is seen in the Northern Volcanic Zone. Ourresults support a model whereby deep melts mix until melt channelization starts in the mantle, after which binary mixing between the homogenized deep melt and shallower fractional melts occurs.

1 Introduction

Iceland is an ideal natural laboratory for studying both active volcanic processes and large-scale tectonic processes. Its location over both the Mid-Atlantic Ridge and a deep-seated mantle plume means that Icelandic magmas sample both shallow and deep mantle domains (Einarsson, 2008). The proposed plume centre lies west of the Vatnajokull ice cap (Lawver and Muller, 1994; Wolfe et al., 1997; Bjarnarson, 2008), where high $^3He/^4He$ ratios up to 25.9 R_A have been measured in subaerial glasses and geothermal fluids (Harðardóttir et al., 2018). Crustal thickness is greatest in central Iceland at ~40 km, reducing to ~20 km in the active rift zones (Darbyshire et al., 1998; Darbyshire et al., 2000a; Darbyshire et al., 2000b, Jenkins et al., 2018).

Iceland's on-axis neovolcanic zones, the Western Volcanic Zone (WVZ), Eastern Volcanic Zone (EVZ) and Northern Volcanic Zone (NVZ) (Figure 1), lie along the sub-aerial manifestation of the Mid-Atlantic Ridge. They typically erupt tholeiitic basalts through a series of *en echelon* fissures that dissect volcanic centres (Hémond et al., 1993). The Snæfellsnes and Snæfell-Öræfajökull flank zones are located away from the zones of active rifting and are associated with lower $^3He/^4He$ ratios (<10 R_A) than central Iceland (Harðardóttir et al., 2018). The South Iceland Volcanic Zone (SIVZ) is a continuation of the EVZ and has slightly higher $^3He/^4He$ ratios than the other flanks (Harðardóttir et al., 2018). The flank zones typically erupt small volumes of transitional to alkali basalts (Hémond et al., 1993; Peate et al., 2010).

The Icelandic mantle has been proposed to contain both enriched and depleted components that are different from depleted mid-ocean ridge basalt (MORB) mantle (DMM) (Meyer et al., 1985; Hémond et al, 1993, Kerr et al, 1995; Fitton et al., 1997, Chauvel and Hémond, 2000; Fitton et al, 2003; Thirlwall et al., 2004). The isotopic compositions of these enriched and depleted components vary from the north to the south of Iceland, suggesting that there are multiple enriched and depleted components intrinsic to the Icelandic mantle (Thirlwall et al, 2004; Kokfelt, 2006; Shorttle et al., 2013). The presence of a depleted component in the Icelandic plume distinct from DMM has been contested by Hanan et al. (2000) who suggested that Icelandic melt compositions can be generated by mixing of two enriched components and typical DMM. Despite the lack of consensus on the nature of the depleted component(s) of the Iceland mantle, there is agreement that one of the isotopically and incompatible trace element-enriched components is recycled oceanic lithosphere (Hanan et al., 2000; Chauvel and Hémond, 2000, Fitton et al., 2003; McKenzie et al., 2004; Thirlwall et al., 2004; Kokfelt et al., 2006; Shorttle and Maclennan, 2011; Shorttle et al, 2014, Halldórsson et al., 2016a; Halldórsson et al. 2016b; Matthews et al., 2016; Brown and Lesher, 2016; Brown et al., 2020; Rasmussen et al., 2020; Harðardóttir et al., 2022).

In addition to isotopic heterogeneity, several authors have investigated the lithological heterogeneity of the Icelandic mantle (Shorttle and Maclennan, 2011; Shorttle et al., 2014; Matthews et al., 2016; Brown et al., 2020). Shorttle et al. (2014) and Matthews et al. (2016) explored a tri-lithological mantle containing lherzolite, refractory harzburgite and pyroxenite as a source for neovolcanic zone magmas. They used measured melt compositions and temperatures to estimate the fraction of melt derived from a pyroxenite source (F_{px}) and required their modelled mantle lithology abundances to match this F_{px} value. They proposed that the Icelandic mantle is comprised of 9-13 % pyroxenite, ≥30 % refractory harzburgite and the remainder depleted lherzolite. Brown et al. (2020) applied an inversion model that requires the abundances and compositions of mantle lithologies to provide a direct match to measured trace element concentrations in erupted basalts. They argue that the trace element compositions of Icelandic melts can be generated without the presence of harzburgite, and indeed the Shorttle et al. (2014) and Matthews et al. (2016) models consider harzburgite to be a non-melting lithology. However, Shorttle et al. (2020) showed that a harzburgite-free mantle would require a potential temperature in excess of any reasonable geochemical estimates (e.g., Matthews et al., 2016, Spice et al., 2016) to produce the observed 20 km crustal thickness of the neovolcanic zones. While these studies estimated the abundance of different lithologies in the bulk Icelandic mantle, the influence of lithological heterogeneity on melt compositions across Iceland is mostly limited to the lengthscale of the neovolcanic zones and has not considered the flank zones (e.g. Shorttle et al., 2014). Rasmussen et al. (2020) used olivine trace element geochemistry to suggest that there is no evidence of a distinct olivine-free pyroxenite lithology in the mantle beneath the Snæfellsnes Flank Zone but did find evidence of a large olivine-bearing pyroxenitic contribution in the SIVZ. Harðardóttir et al. (2022) show that isotopic heterogeneity in Icelandic volcanic rocks relies on lithospheric thickness, with the flank zones preferentially sampling low-degree melts from geochemically enriched “blobs” of recycled origin.

The heterogeneous nature of the Icelandic mantle has given rise to striking heterogeneity in the chemical composition of erupted basalts in Iceland. Geochemical variability across a range of scales can be produced by channelized flow in the mantle, where melts are transported rapidly to the surface and compositions produced at depth are preserved (Spiegelman and Keleman, 2003; Weatherley and Katz, 2012; Rudge et al., 2013). Most evidence for channelization in the mantle comes from observations from ophiolites and numerical studies (Kelemen et al., 1995; Kelemen and Dick, 1995; Suhr et al., 1999; Kelemen et al., 2000; Spiegelman et al., 2001; Spiegelman et al., 2003; Liang et al., 2010; Liang et al., 2011; Weatherley and Katz, 2012). The aims of our study are to better understand how the different lithologies' contributions to erupted melts vary across Iceland, how melting processes and transport affect erupted melt compositions and how this information on melting and mixing processes are recorded in the melt inclusion record.

To explore how different mantle lithologies contribute to melt compositions across Iceland we have applied melt modelling to reproduce the trace element compositions measured in olivine- and plagioclase-hosted melt inclusions from individual eruptions located in Iceland's active neovolcanic zones and flank zones. We used REEBOX Pro (Brown and Lesher, 2014; Brown et al. 2020) to model the melting of a lithologically heterogeneous mantle. Outputs from REEBOX Pro were then used to assess if observed melt inclusions could be matched by aggregate melt composition and if channelized transport occurs following homogenization or if input from shallower melts is required to produce the observed compositions input to melt mixing models to quantify the relative contributions of different mantle sources to melt production in thirteen localities for which melt inclusion data are available. Our results suggest that channelization in the mantle and rapid transport of a deep homogenized melt fits melt compositions in the majority of Iceland's flank zones, though there is some variation in the threshold for onset of this channelization. In the rift zones aggregate deep melts cannot match the observed compositions and further mixing with shallower melts is required.

2 Materials and Methods

2.1 Sampling, sample preparation and compilation of melt inclusion literature data

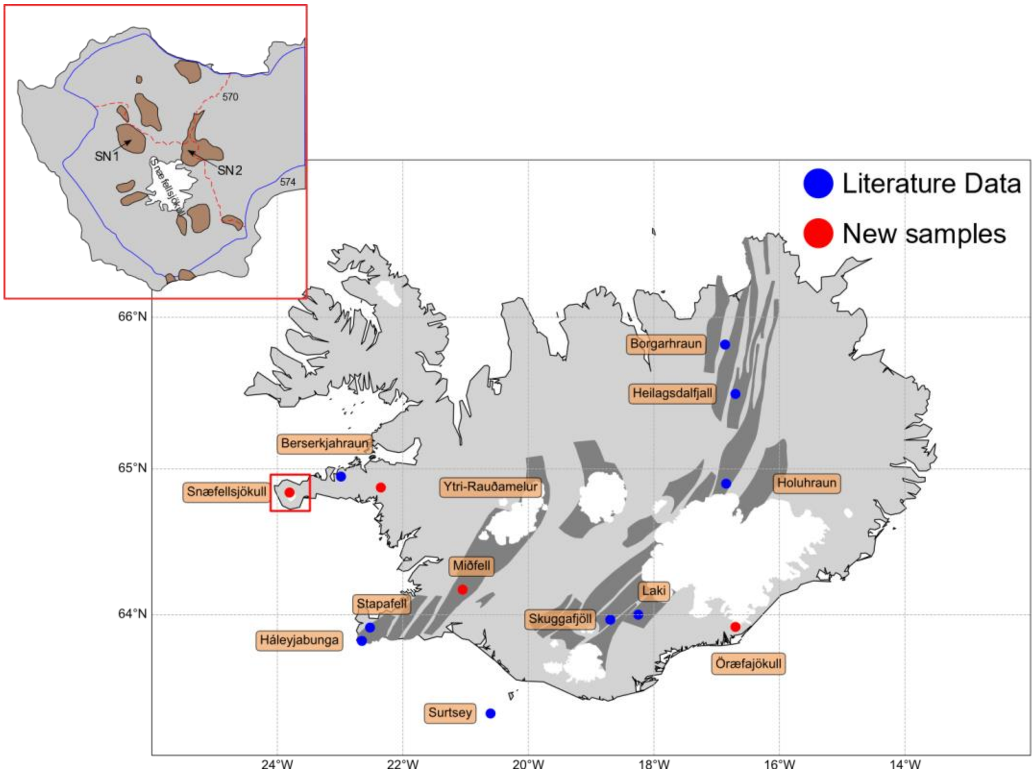

Figure 1: Map of Iceland showing the locations of samples collected as part of this study (Snæfellsjökull, Ytri-Rauðamelur, Öræfajökull, and Miðfell) and of compiled literature melt inclusion data. Volcanic systems are highlighted in dark grey and mark the extent of the neovolcanic zones. SFZ – Snæfellsnes Flank Zone, SÖFZ – Snæfell-Öræfajökull Flank Zone, SIVZ – South Iceland Volcanic Zone, NVZ – Northern Volcanic Zone, EVZ – Eastern Volcanic Zone, WVZ – Western Volcanic Zone. The red box shows a detailed map of Snæfellsjökull and sample locations. Subglacial eruptions are shown in brown, glacier in white. Roads are represented by blue and red lines. Samples collected are referred to as SN1 and SN2.

Our samples comprise glassy rinds of subglacial pillow lavas and glassy hyaloclastite fragments. We sampled three localities that allow us to investigate lithological variations along a transect across the Icelandic mantle (Figure 1): (1) The Snæfellsnes Flank Zone, far from the plume centre and active rifting; (2) Miðfell, in the active Western Volcanic Zone; and (3) Öræfajökull, a flank zone closer to the active rifts and close to the plume centre.

Snæfellsjökull is a volcanic centre located at the western tip of the Snæfellsnes Peninsula. The thick lithospheric lid (Table 1) above the Snæfellsnes Flank Zone results in less adiabatic decompression melting than beneath the neovolcanic rift zones, and thus small volumes of relatively enriched melts are generated (Peate et al., 2010). We collected samples of glassy pillow rims from two subglacial basalt eruptive units around the Snæfellsjökull volcanic centre (Figure 2), henceforth referred to as SN1 and SN2, and one sample of olivine-phyric basaltic scoria from Ytri-Rauðamelur, located further inland on the Snæfellsnes Peninsula.

Miðfell is located in the Western Volcanic Zone (WVZ) within the Hengill volcanic system (Figure 1). It comprises Late Glacial glassy olivine- plagioclase-, clinopyroxene- and gabbroic nodule-phyric pillow lavas and hyaloclastites (Guernko and Chaussidon, 1995; Gurenko and Sobolev, 2006). Previous studies of olivine-hosted melt inclusions from Miðfell have revealed both enriched and depleted incompatible trace element (ITE) signatures relative to primitive mantle (Guernko and Chaussidon, 1995; Gurenko and Sobolev, 2006; Miller et al, 2019), making Miðfell an ideal location for investigating mantle heterogeneity on the lengthscale of an individual eruption. Basaltic glass sample DICE10 from Miðfell has higher $^{20}Ne/^{22}Ne$ and lower $^{129}Xe/^{130}Xe$ than MORB mantle, suggesting that this eruption sampled a near-primordial mantle component that has remained largely unmodified and undegassed since ~4.45 Ga (Harrison et al., 1999; Mukhopadhyay, 2012).

Öræfajökull, located beneath the southern tip of the Vatnajökull glacier, forms the southern end of the Snæfell-Öræfajökull Flank Zone, approximately 50 km from active rifting (Roberts and Gudmundsson, 2015). Öræfajökull has erupted subglacial basaltic pillow lavas and hyaloclastites, as well as rhyolitic lavas and pyroclastic deposits. Low $^{143}Nd/^{144}Nd$ and high $^{208}Pb/^{204}Pb$ and $^{87}Sr/^{86}Sr$ ratios compared to the rift zones suggest the presence of an EM-type mantle beneath Öræfajökull (Prestvik et al., 2001, Kokfelt et al., 2006, Manning and Thirlwall, 2014). Notably low $^{3}He/^{4}He$ ratios suggest that there is limited role of undegassed components of the mantle plume in Öræfajökull (Harðardóttir et al., 2018) We sampled olivine- and plagioclase-phyric glassy hyaloclastite from the western side of Öræfajökull (Figure 1).

Samples were hand-crushed and olivine and/or plagioclase macrocrysts containing glassy melt inclusions were hand-picked under a binocular microscope. The macrocrysts were typically around 3-7 mm in their longest dimension and were all fresh bar some minor surface alteration of olivines from Öræfajökull. The melt inclusions were glassy with no daughter crystals and ranged from 50 to 300 μm in length. A small number of inclusions contained vapour bubbles. The olivines host individual isolated inclusions, whereas the plagioclases contain groups of melt inclusions. Individual crystals were polished to expose melt inclusions at the surface, then mounted in epoxy and polished to a flat surface for analysis.

We have supplemented our samples with literature melt inclusion data from across Iceland (Figure 1). This provides us greater spatial coverage with which to investigate the relative contributions of mantle domains to melt generation across Iceland. The additional locations are Stapafell (Matthews et al., 2021), Hàleyjabunga (Matthews et al., 2021), Skuggafjöll (Neave et al., 2014), Laki (Neave et al., 2013), Holuhraun (Hartley et al., 2018), Heilagsdalsfjall (Matthews et al., 2021) and Borgarhraun (Hauri et al., 2018) in the neovolcanic zones, and Surtsey (Schipper et al., 2016) and Berserkjahraun (Matthews et al., 2021) in the flank zones. We also used Miðfell olivine-hosted melt inclusion compositions (Miller et al. (2019)) to supplement our own data from that eruption.

2.2 Electron Probe Microanalysis (EPMA)

Snæfellsjökull, Öræfajökull and Miðfell: The major element compositions of melt inclusions, their host crystals and glasses were analysed by EPMA at the University of Manchester and University of Bristol using Cameca SX100 electron microprobes. Melt inclusions and glasses were analysed over three sessions, two at the University of Manchester and one at the University of Bristol. The first session at the University of Manchester used a 15kV, 3 nA, 15 μm diameter beam for all elements. The second session used a defocused 20 μm beam and two column conditions: the first measured Fe, Mn, S, K, Ca, P, Ti, Na, and Mg at 10 nA followed by a second condition which measured Al and Si at 2 nA. At the University of Bristol, melt inclusions were measured with a 10 μm diameter, 20 nA beam at 20 kV. An additional glass (EWB6) was measured in a subsequent session at the University of Bristol. In this session two beam conditions were used: Si, Ca, Al, Na, P and Fe were measured first using a 15 kV, 10nA, 5µm beam followed by a second column condition which measured Cr, Mn, S, Cl, F, Mg and Ti with a 15 kV, 5 µm beam. In all the analytical sessions, Na was measured first to prevent migration under the beam. Precision and accuracy were monitored by repeat analysis of NMNH basaltic glass standards A99, VG2 and 113716 (Jarosewich et al., 1980) and BCR2 (Wilson, 1997).

Olivine and plagioclase macrocrysts were analysed during two sessions at the University of Manchester using a 1 µm, 15 kV beam. For olivine, two beam conditions were used: major elements (Fe, Mg and Si) were measured first using a beam current of 5 nA, and trace elements (Ca, Na, Co, Ni, Mn, Cr, P, Ti and Al) were measured second using a 40 nA beam. For plagioclase, a beam current of 10 nA was used to measure Ca, K, Al, Na and Si, followed by a current of 100 nA for Fe, Ti, Mg and P. Olivines and plagioclases measured at the University of Bristol were analysed with a focused 1 µm 20 kV electron beam. For olivine, two column conditions were used: first a 20 nA beam to measure Mg, Si, Ca, Mn, Fe, Ca and Ni, and then a 100 nA beam to measure Al, P, Ti, Cr and Co. Plagioclases were measured using one column condition with a 20 nA beam current. Olivine and plagioclase internal standards were measured during analysis to monitor accuracy and precision.

Ytri-Rauðamelur: Major element contents of olivine macrocrysts and melt inclusions were measured by EPMA using a Cameca SX100 at the University of Cambridge following the methodology of Neave et al. (2018). Glass hosting the macrocrysts was rehomogenized and measured alongside the melt inclusions to check precision on a composition as close as possible to that of the melt inclusions.

2.3 Secondary Ion Mass Spectrometry (SIMS)

Snæfellsjökull, Oræfajökull and Miðfell: Selected trace and rare earth elements (REEs) were obtained from 93 melt inclusions (46 from Snæfellsjökull, 40 from Miðfell and 7 from Öræfajökull) were measured using the Cameca ims-4f secondary ion mass spectrometer at the NERC Ion Microprobe Facility, University of Edinburgh. The following isotopes of each element were measured (count time in seconds in parentheses): ^{1}H (3), ^{7}Li (2), ^{11}B (5), ^{19}F (5), ^{26}Mg (2), ^{30}Si (2), ^{35}Cl (2), ^{39}K (2), ^{47}Ti (2), ^{8}Sr (2), ^{89}Y (2), ^{90}Zr (2), ^{93}Nb (5), ^{138}Ba (2), ^{139}La

(2), ^{140}Ce (2), ^{141}Pr (5), ^{142}Nd (5), ^{149}Sm (8), ^{153}Eu (5), ^{157}Gd (5), ^{159}Tb (5), ^{161}Dy (5), ^{165}Ho (5), ^{166}Er (5), ^{169}Tm (5), ^{171}Yb (8), ^{175}Lu (8). Samples were gold-coated prior to analysis. All analyses were carried out with an O^- primary beam with a primary accelerating voltage of 10 kV and secondary accelerating voltage of 4.5 kV minus a 75 eV offset and 25 µm image field. Measurements were calibrated using repeat analysis of GSD basaltic glass (Jochum et al., 2006). Counts were normalised to ^{30}Si, and absolute elemental concentrations were calculated by normalising ^{30}Si to the SiO_2 content determined by EPMA.

Initial analyses measured all the above listed isotopes using a primary beam intensity of 6.9-3.5 nA. The ion beam was rastered for 4 minutes to remove surface contamination. Peak positions were verified during beam rastering. After 4 minutes, isotopes were counted over 10 cycles. Initial results revealed H_2O concentrations <1000 ppm, close to the detection limit. We therefore modified the procedure and subsequently analysed inclusions under two different routines: one for volatiles and light trace elements, and one for heavy trace elements and rare earth elements. Major elements (^{30}Si, ^{26}Mg, ^{39}K, ^{47}Ti) were included in both routines to ensure consistency. In all analyses the background was monitored by measuring masses 0.7 (1) and 130.5 (5) and was negligible.

Lighter isotopes (^{1}H, ^{7}Li, ^{11}B, ^{19}F, ^{35}Cl) were measured first, with a primary beam condition of 4-10 nA. The ion beam was rastered for 4 minutes before analysis. After rastering, each mass was measured sequentially over 20 cycles, with the final 10 used to calculate element concentrations.

Heavy trace elements (^{88}Sr, ^{89}Y, ^{90}Zr, ^{93}Nb, ^{138}Ba, ^{139}La, ^{140}Ce, ^{141}Pr, ^{142}Nd, ^{149}Sm, ^{153}Eu, ^{157}Gd, ^{159}Tb, ^{161}Dy, ^{165}Ho, ^{166}Er, ^{169}Tm, ^{171}Yb, ^{175}Lu) were measured second, in the same spots as the light trace element analyses. Measurements were made using a primary beam of 4-9 nA. The ion beam was rastered for 1 minute, during which peak positions were verified. Elements were measured over 10 cycles, and all cycles were used to calculate element concentrations.

Precision and accuracy of trace element analyses were monitored by repeat measurements of MPI-DING silicate glass standards StHs/80-G, ML3B-2and KL2-G (Jochum et al., 2006), and N72, M5, M10 and M24 (Shishkina et al., 2010). Precision is calculated from repeat analysis of all standards. Accuracy is based on repeat measurements of KL2-G as this standard is compositionally most similar to the unknowns. Elements with low abundance in KL2-G return low accuracy (±20% or greater), which reflects scatter around a low concentration rather than poor analyses.

H_2O concentrations were determined by a calibration curve created with measurements of standards GSD, StHs/80-G , N72, M5 , M10 and M47, all with known H_2O contents (Jochum et al., 2006, 2011; Shishkina et al., 2010). Precision and accuracy were calculated based on hydrous standards M5, M10 and M47 which contain >1000 ppm H_2O. Precision was better than ±3 % and accuracy better than ±14 %.

Ytri-Rauðamelur: Trace element contents of melt inclusions were measured by SIMS using a Cameca imf-5f at the Institute of the Earth's Interior at Okayama University, Japan following the methodology of Neave et al. (2018).

All EPMA and SIMS compositional data are provided as supporting information.

2.4 REEBOX Modelling

REEBOX Pro (Brown and Lesher, 2016; Brown et al., 2020) is a stand-alone software package that can be used to model mantle melting in a rifting environment. The strength of REEBOX is its ability to model the melting of more than two mantle components to calculate instantaneous and column accumulate melt compositions over a range of pressures and temperatures. A maximum of 6 lithologies are available to input: hydrous lherzolite, anhydrous lherzolite, harzburgite, and three different pyroxenite compositions: G2 (silica-saturated MORB-like pyroxenite; Pertermann and Hirschmann, 2003), MIX1G (silica-undersaturated garnet pyroxenite; Hirschmann et al., 2003) and KG1 (50:50 MORB and peridotite mix; Kogiso et al., 1998). The user must input the desired mantle lithologies and their proportions, as well as the mantle potential temperature, spreading rate, pre-existing lithosphere thickness, and the style of rifting. The pressure and temperature of melting are incrementally reduced during the calculation, and output melt compositions are produced for each pressure step.

We used REEBOX Pro to model melting of a lithologically heterogeneous mantle beneath Iceland. The starting composition of the mantle was 60% anhydrous peridotite of DMM composition (Salters and Stracke, 2004), 30% harzburgite (Salters and Stracke, 2004) and 10% KG1 pyroxenite (E-MORB composition), with lithology proportions derived from Shorttle et al.

(2014) and Matthews et al. (2016). The harzburgite fraction is set to be a non-melting component (Matthews et al., 2016, Shorttle et al., 2014), but its presence does affect the productivity of the other melting lithologies through its buffering of mantle temperature during melting. We selected KG1 pyroxenite as this has previously been shown to be a good estimate for the pyroxenite present in the Icelandic mantle (Shorttle et al. 2014, Shorttle and Maclennan, 2011), although choosing G2 or MIX1G pyroxenites does not produce significant variations in the trace element signatures of the bulk crust generated from melting (Brown et al., 2020). We selected a mantle potential temperature of 1480°C (Matthews et al., 2016) for all sample areas, and half spreading rate of 0.1 cm/yr (Karson et al., 2017). We estimate the pre-existing lithosphere thickness in each location based on the thicknesses of crust and lithospheric mantle lid determined by Bjarnason and Schmeling (2009). Lithospheric thicknesses for the flank zones were estimated based on measurements for Northwest Iceland. Lithospheric thicknesses for Western Volcanic Zone were based on measurements from West Iceland, and lithospheric thicknesses for the Eastern and Northern Volcanic Zones were based on the Central Iceland Line (Table 1). Densities of the crust and mantle lithosphere were estimated following Staples et al. (1997).

Area	Crustal thickness (km)	Mantle Lid thickness (km)	Crustal density (kg/m^3)	Mantle density (kg/m^3)
Flank zones	24	41	2400	3240
WVZ	19	11	2400	3170
EVZ, NVZ	20	20	2400	3170

Table 1: Lithospheric thicknesses from Bjarnason and Schmeling (2009) and densities from Staples et al. (1997) used for different sample areas in our modelling

We processed the outputs from REEBOX Pro as follows. All output column accumulate (aggregate) melt compositions across the full range of melting pressures and temperatures were compared to the mean measured trace element compositions of melt inclusions from each sample area. The mean trace element concentration was determined for the elements modelled in each system and these are illustrated in the supporting information. Acceptable matches were identified through chi-squared misfit calculations. The chi-squared misfit for each model result was calculated as follows:

$$\chi^2 = \sum \left[\frac{x_i - \mu_i}{\sigma_i}\right]^2,$$

where x_i is the mean PEC-corrected concentration of element *i* in the sample, σ_i is one standard deviation of the concentration of the element across all measurements and μ_i the concentration of each element in the modelled melt. The mean composition is taken as an average of the melt inclusion compositions from each eruption and the standard deviation reflects the variability in melt inclusion composition within an eruption. Modelled melt compositions were accepted as a potential fit if the chi-squared misfit was below the critical value according to the number of degrees of freedom in the system (number of elements minus one) for a p-value of 0.05.

Matching between modelled aggregate (column-accumulated) melts and measured melt inclusion compositions returned acceptable fits for the three Snæfellsnes Peninsula localities and Surtsey, but not for the other locations. The Snæfellsnes Peninsula and Surtsey are distinct from the neovolcanic zone localities in having thicker lithosphere that restricts melting to high pressure and low degrees (Peate et al., 2010). The modelled aggregate melt composition that match those observed in the Snæfellsnes Peninsula and Surtsey are produced my mixing of pyroxenite- and lherzolite-derived melts derived when lherzolite has undergone only low degrees of melting. The homogenized melt produced by the model are analogous to the model of Rudge et al. (2013), who proposed that a deep melt component is created beneath Iceland by mixing pyroxenite- and lherzolite-derived melts produced before lherzolite has undergone 5 % melting. This deep melt component then mixes with shallower lherzolite- and pyroxenite-derived melts as it moves through the mantle column, producing the more depleted melt compositions of the neovolcanic zones (Rudge et al., 2013). Therefore, to fit the compositions of the neovolcanic zones and Öræfajökull Flank Zone we adapted the model described above. Rather than taking aggregate homogenized melts from the melting region, we adopt the model proposed by Rudge et al. (2013) and consider mixing between deep and shallow melts (Figure 2).

For the deep melt, we use the aggregate melt composition from REEBOX that best fits the mean composition of Snæfellsjökull melt inclusions. We then mix this deep melt component with the instantaneous melt compositions for lherzolite-derived melts produced by greater than 5% melting. Instantaneous melts are produced at intervals of 0.01 GPa. For simplicity, we did not include shallower pyroxenite-derived melts in the mixing model. This is because shallower pyroxenites have already undergone high degrees of melt extraction and are depleted in incompatible trace elements; therefore, additional instantaneous pyroxenite-derived melts have negligible effect on the incompatible trace element budget of the mixed melt (e.g., Rudge et al. 2013). During the deep-shallow melt mixing we vary the degree to which the shallower lherzolite-derived melts have been aggregated, from mixing with individual instantaneous melts to homogenising large groupings of the instantaneous melts. Homogenization was calculated over pressure intervals of 0.03, 0.05, 0.07, 0.10, 0.15, 0.20, 0.25, 0.50, 1.00, 1.50 GPa in extent throughout the melting region (Figure 3). The mixing ratio between the deep melt component and shallower lherzolite melts to each mixed melt composition was varied in 5% increments from 0 to 100%.

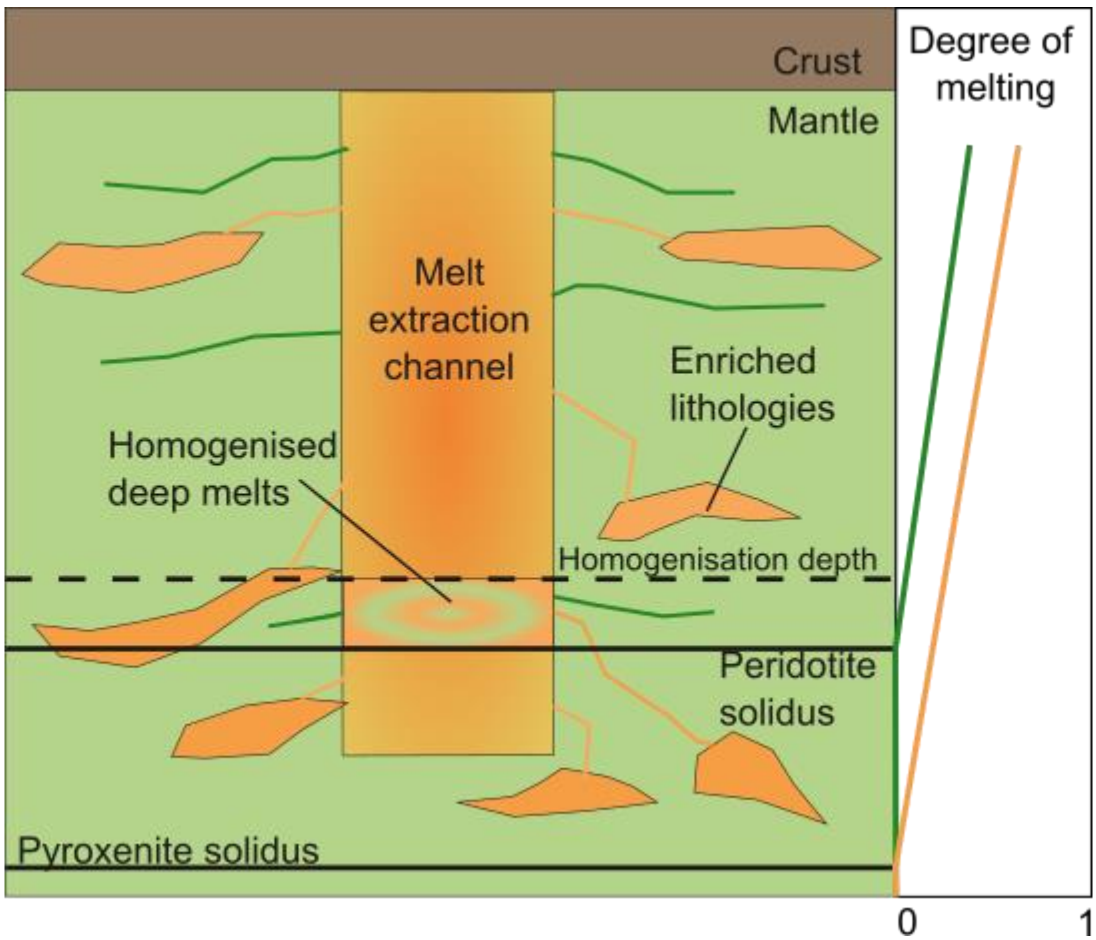

Figure 2: Schematic diagram of the melt mixing model of Rudge et al. (2013). Low-degree melts of lherzolite and higher degree melts of pyroxenite homogenise at depth in the mantle, before ~5% melting of the lherzolite has been reached. Above this point, the deep homogenized melt mixes with higher-degree instantaneous or aggregated melts of lherzolite and pyroxenite in the melt extraction channel.

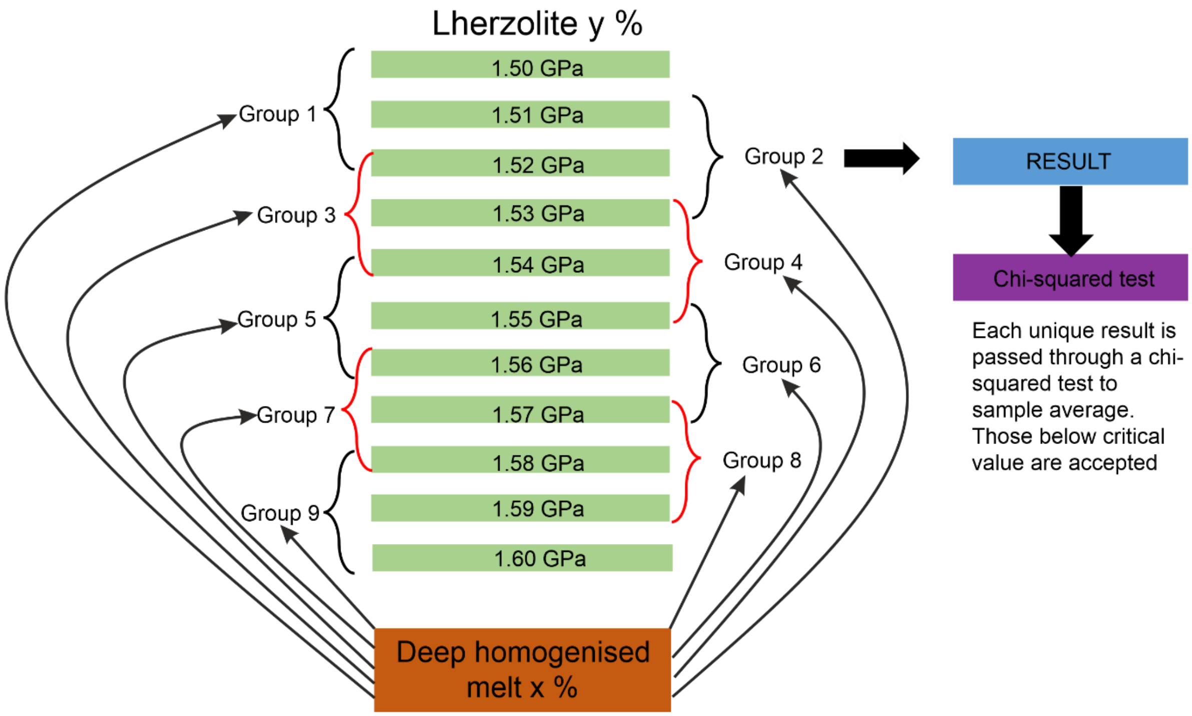

Figure 3: Flowchart through the secondary melt mixing model. X and Y represent the percentage input of melts from the deep homogenized melt and shallower lherzolite melts to the mixed composition. The groups show the homogenization intervals, here spanning 0.03GPa of melt generation. The pressures of the lherzolite melts are for illustrative purposes and do not show all lherzolite instantaneous melts included in the calculation. Thin arrows represent mixing between the deep homogenized melt and the homogenized instantaneous melts.

In running the model, first the mixing ratio between deep homogenized melt and shallower lherzolite melts is set. A specific pressure interval of lherzolite instantaneous melts is selected and homogenized. This is then mixed, in the defined ratio, with the homogenized deep melt component. Each mixture involving a distinct homogenized group of lherzolite melts produces a unique result for comparison with the observations. Once all deep-shallow mixtures have been explored, the model changes the mixing ratio between deep and shallow melts and the process starts again. The model is run for each size of homogenization interval for the lherzolite instantaneous melts. Figure 3 illustrates the selection and mixing of melts as a flowchart.

Thirteen trace element concentrations (Nb, La, Ce, Pr, Nd, Sm, Eu, Gd, Dy, Y, Er, Yb, Lu) were used to compare the measured and modelled melt compositions. Acceptable fits were returned when the chi-squared misfit was below critical chi-squared value for a 13-component system with a p-value of 0.05 (21.03). Borgarhraun literature data do not include Lu or Pr, so these elements were excluded from Borgarhraun models and the critical chi-squared value altered to 18.31 to reflect the change to an 11-component system. Literature data for Surtsey exclude several of the elements selected for the model so we replaced missing elements with different elements that had been analysed, keeping the total at 13 elements. Acceptable fits were returned for all sample areas except Skuggafjöll and Öraefajökull. Skuggafjöll melt compositions possess small anomalies in Nd, Sm, Gd and Eu concentrations when normalised to primitive mantle. These elements were removed from the comparison, and an acceptable fit was achieved with this reduced system, with the critical chi-squared value of 15.51 for a 9-component system. For Öraefajökull we explored different combination of elements and changes in melting regime but did not find any acceptable fit. Thus, we present the best fit found for Öraefajökull for the 13-element system using lherzolite-derived melts from both the modelled EVZ and flank zone melting regimes.

3 Results

3.1 Host mineral compositions

In all our samples, melt inclusion-bearing olivine and plagioclase crystals are relatively primitive in composition. Miðfell olivines vary from 81.7 to 90.1 mol% Fo, with an average composition of Fo_{87} and all but three crystals being more primitive than Fo_{86}. Snæfellsjökull olivines range from 79.4 to 87.2 mol% Fo, with an average composition of Fo_{84}. Snæfellsjökull plagioclases range from 78.9 to 86.8 mol% An with an average composition of An_{83}. Olivines from Ytri-

Rauðamelur range from 83.3 to 88.8 mol% Fo, with an average composition of Fo_{87}. Öræfajökull has the least primitive olivines ranging from 81.4 to 83.2 mol% Fo.

3.2 Melt inclusion major element compositions

Melt inclusions experience post-entrapment crystallisation (PEC) where the host mineral crystallizes on the wall of the inclusion following trapping (e.g., Kent, 2008). Olivine-hosted melt inclusions were corrected for PEC and diffusive loss of Fe using Petrolog3 (Danyushevsky and Plechov, 2011). For each melt inclusion, we determined the expected FeO content at the time of inclusion trapping using the relationship between TiO_2 and FeO wt% for a liquid line of descent derived from literature measurements of basaltic glass compositions in the sample area. For Miðfell, PEC corrections of 0.2-18.4% olivine addition were required, with a mean correction of 6.0%. Seven inclusions required olivine removal from the measured melt composition; four of these inclusions have MgO ~9 wt% and required <1% removal of olivine. Three low-MgO inclusions required 10.3-12.0% removal of olivine. Olivine removal indicates that the host crystal was heated above the temperature of inclusion trapping, causing the host crystal to melt and increase the Mg# of the melt inclusion composition (Danyushevsky and Plechov, 2011). Olivine-hosted inclusions from Öræfajökull required PEC corrections between 15.2-25.4% olivine addition, with a mean correction of 21.1%. Olivine-hosted inclusions from Ytri-Rauðamelur required 5.4-30.6% olivine addition, with a mean correction of 14.2%. Olivine-hosted inclusions from the two Snæfellsjökull samples required 1.6-17.6% olivine addition, with a mean correction of 9.6%; one inclusion required 1.4% removal of olivine from the measured composition.

Plagioclase-hosted melt inclusions from Snæfellsjökull were corrected for PEC using the method of Neave et al. (2017). Equilibrium plagioclase composition is added back into the melt inclusion until its Al_2O_3 content matches the liquid line of descent predicted from Al_2O_3-MgO systematics of basalts and basaltic glasses from the Snæfellsnes Flank Zone. These inclusions required PEC corrections of <10%. Additional details of PEC calculations are available in the supporting information.

PEC-corrected major element compositions of our melt inclusions are presented in Figure 4. Olivine-hosted melt inclusions from Miðfell typically contain between 9.1 and 13.4 wt% MgO, except for three inclusions with 6.0-6.8 wt% MgO. Öræfajökull melt inclusions are generally more evolved, containing 8.8-10.6 wt% MgO. Melt inclusions in the two samples from Snæfellsjökull have different compositions. The first sample, SN1, is plagioclase-phyric, and the plagioclase-hosted melt inclusions contain 4.9-6.9 wt% MgO. The second sample, SN2, is olivine-phyric, and its melt inclusions are more primitive, containing 7.5-12.7 wt% MgO. Ytri-Rauðamelur melt inclusions have similar MgO contents to SN2, varying between 8.1 and 13.5 wt% MgO. Melt inclusions from the flank zones are more alkalic than those from Miðfell, with Snæfellsjökull being the most enriched in K_2O. Inclusions from sample SN1 have distinctive high Na_2O concentrations of up to 4.9 wt%. All samples except SN1 have remarkably primitive melt compositions. They should therefore have undergone minimal crustal processing and closely resemble near-primary mantle-derived melt compositions.

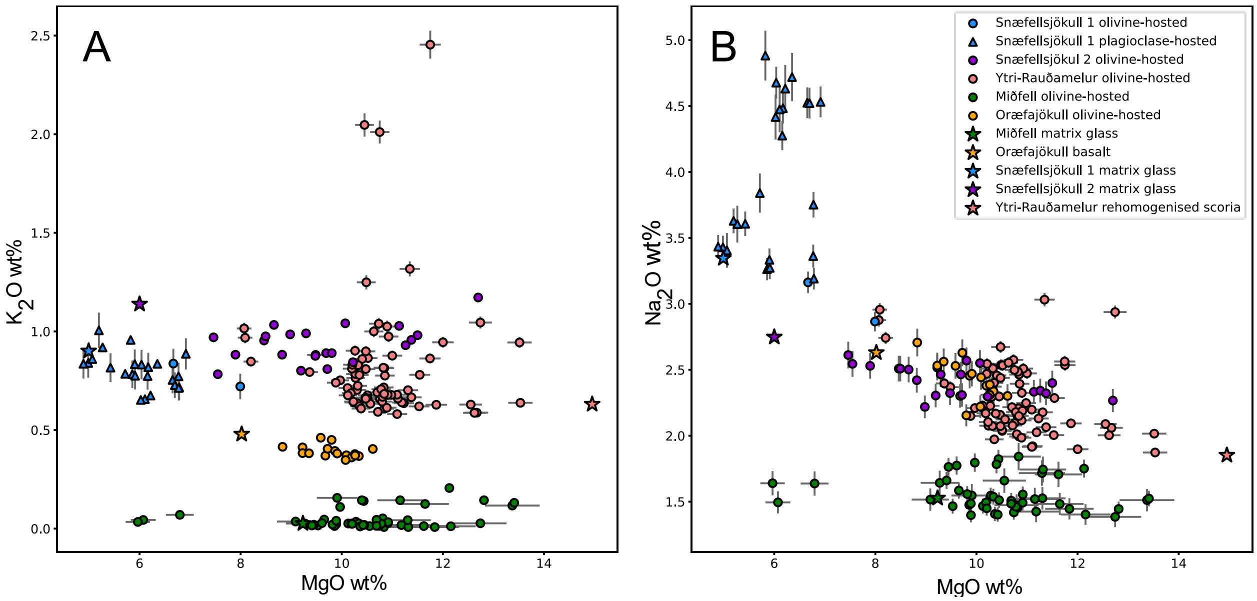

Figure 4: PEC-corrected major element compositions of crystal-hosted melt inclusions from Iceland. Stars show the matrix glass compositions for the samples from Snæfellsjökull 1 (SN1), Snæfellsjokull 2 (SN2) and Miðfell or, for Ytri-Rauðamelur, the composition of glass made from rehomogenized scoria. For Oræfajökull, the star is a basalt from a nearby location to our samples (Manning and Thirlwall, 2014). Uncertainty shown as 1σ external error from precision on secondary standards.

3.3 Melt inclusion trace element compositions

Melt inclusion trace element compositions were corrected for PEC using partition coefficients collated from O'Neill and Jenner (2012), McKenzie and O'Nions (1991), Marschall et al. (2017), Beattie (1994), Nikogosian and Sobolev (1997), and Schnetzler and Philpotts (1970). Corrected trace element compositions for all samples are presented as multi-element plots normalized to the primitive mantle values of Sun and McDonough (1989) (Figure 5). Samples from the Snæfellsnes Flank Zone are particularly enriched in the most incompatible trace elements (Ba and Nb). Öræfajökull melt inclusions are somewhat less enriched in the most incompatible trace elements than Snæfellsnes samples. Miðfell melt inclusions fall into two compositional groups. The first group show mild enrichment in the most incompatible trace elements. The second group is depleted in the most incompatible trace elements. The positive Sr and negative Nd anomalies in the Miðfell melt inclusions have been observed previously and may be the result of melts interacting with gabbroic crust during ascent (Gurenko and Sobolev, 2006; Miller et al., 2019). These elements are therefore not considered when trying to model source contributions.

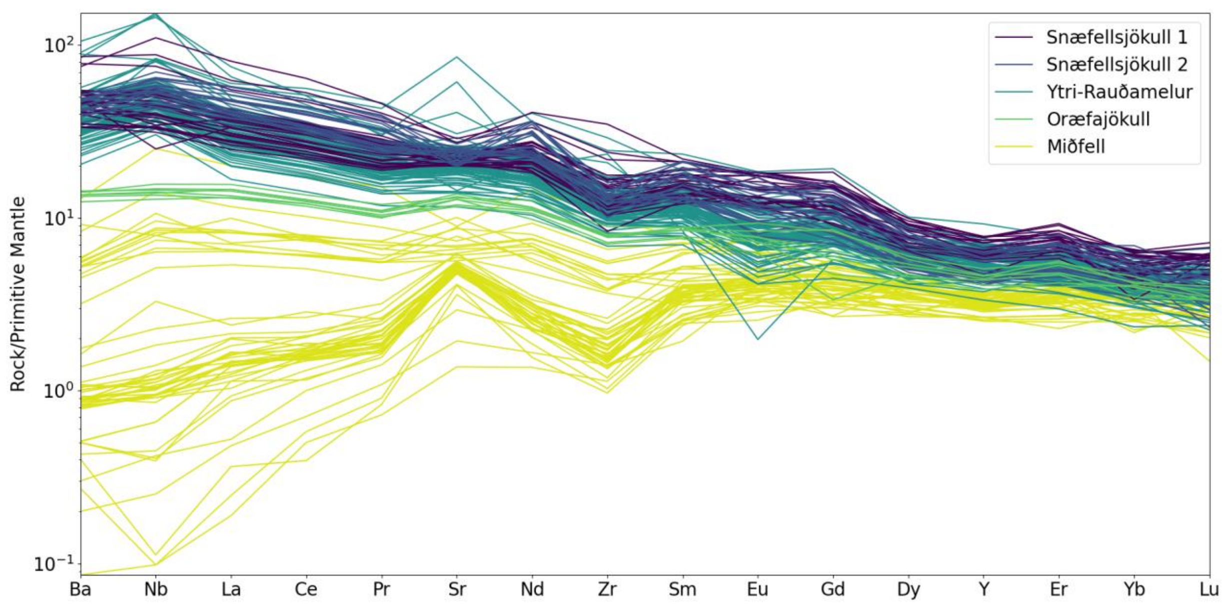

Figure 5: Multi-element plot of melt inclusions from Iceland. All compositions are normalized to primitive mantle (Sun and McDonough, 1989).

Figure 6 shows Zr/Nb vs Ce/Y for the two Snæfellsjökull samples SN1 and SN2. Hardarson and Fitton (1991) used these trace element ratios to define compositional differences between early-, late- and post-glacial volcanism in the Snæfellsjökull volcanic centre. The melt inclusions plot in two distinct clusters (Figure 6). Plagioclase-dominated sample SN1 clusters within the range of late glacial melts from the volcanic centre. The few outliers from this range, with higher Ce/Y, may be inclusions formed towards the end of the late glacial period when melting began to shift towards greater depths. Olivine-dominated sample SN2 clusters within the range of early glacial melts. Both the early glacial and postglacial melts are proposed to have been produced by >2% partial melting near the garnet-spinel transition based on whole-rock trace element compositions. Retreat of the 2 km-thick glacier during the late glacial period resulted in isostatic rebound, and an associated small increase in the degree of melting and a shift towards spinel lherzolite melting (Hardarson and Fitton, 1991). SN2 inclusions may have been erupted earlier and the shift in composition to SN1 reflective of melting of the mantle source at lower pressures.

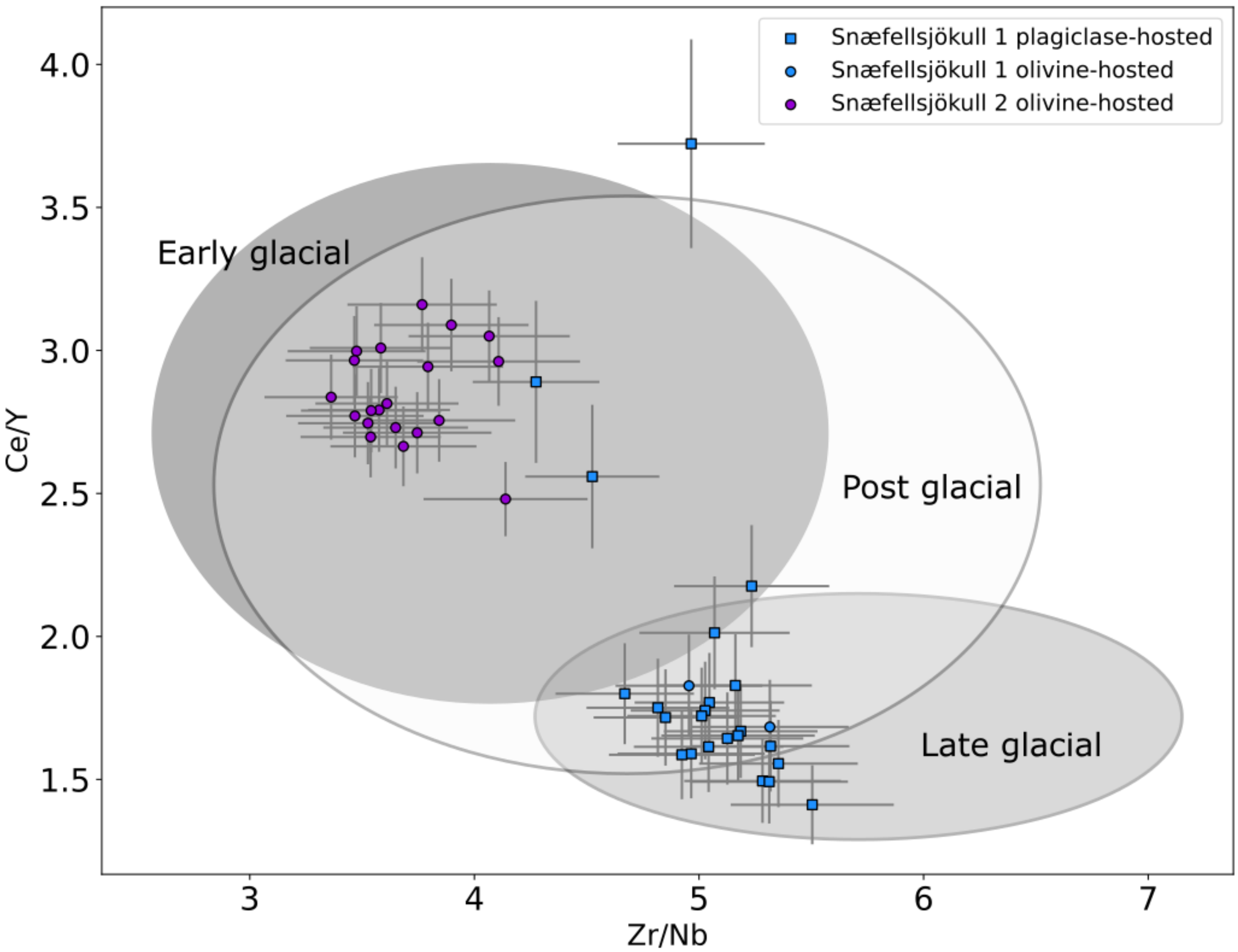

Figure 6 - Zr/Nb vs. Ce/Y for melt inclusions from the Snæfellsjökull. The stars show the average compositions of Early, Late and Post-Glacial basalts from Snæfellsjökull (Hardarson and Fitton, 1991), with 1σ error bars.

3.4 Melting under Iceland's flank zones

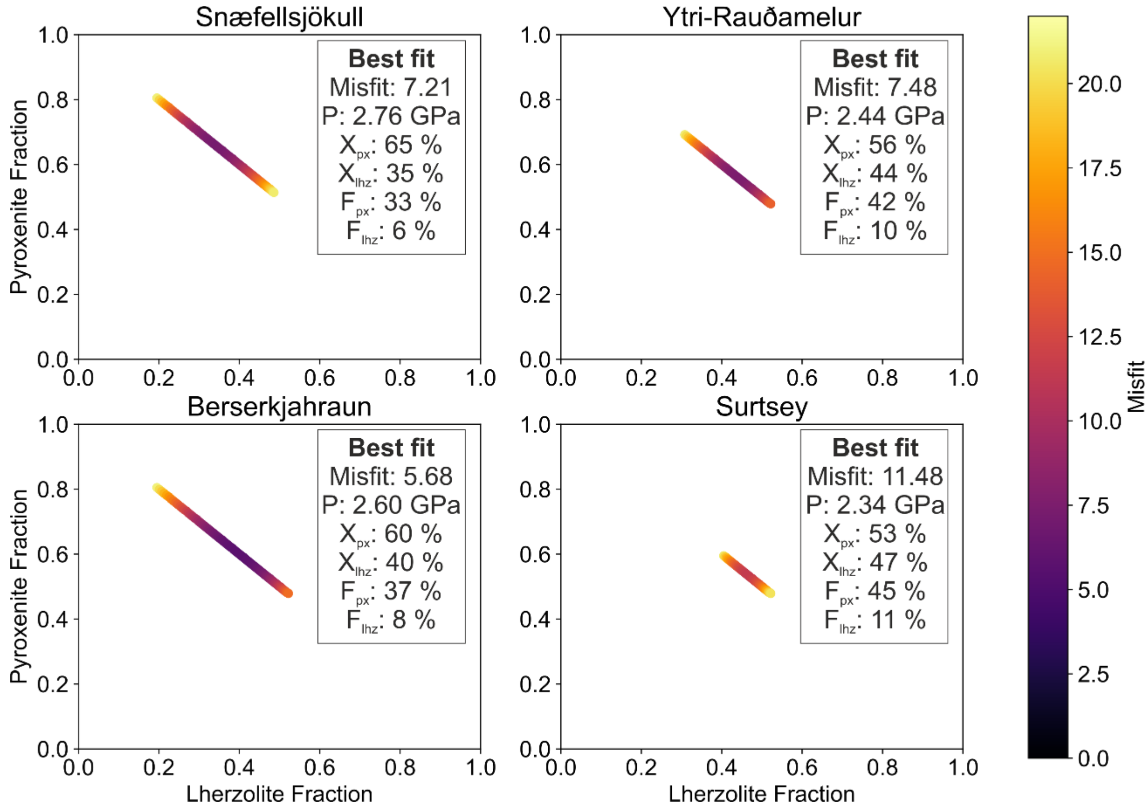

Figure 7: Misfit results for homogenized melts for flank zones. Fractions on axes refer to the fraction of melts from each lithology in the homogenized melts. Only results with misfits below the critical chi-squared value (21.03) are displayed. Details of the best fit model melt composition for each area is detailed in an internal box. X refers to the contribution of melts from each lithology to the homogenized melts. F refers to the fraction of melting undergone by each lithology. P refers to the pressure at the top of the melting column from which melts are homogenized. Px = pyroxenite, lhz = lherzolite.

The following section compares the results of the output column accumulate (aggregate/ homogenized) melts from REEBOX Pro with measured and compiled literature melt inclusion compositions from the flank zones. The output melt compositions from REEBOX represent melts produced by homogenization of all instantaneous melts of lherzolite and pyroxenite below a given pressure. Öræfajökull melt inclusion compositions could not be matched by any homogenized melt component; this location is discussed separately in Section 3.7.

The misfit of the modelled compositions to the melt inclusion compositions of the flank zones are detailed in Figure 7. Modelled homogenized melt compositions return acceptable fits to the mean PEC-corrected melt inclusion composition for Snæfellsjökull, Ytri-Rauðamelur, Berserkjahraun and Surtsey. An average for Snæfefellsjökull was determined from combining the compositions of both eruptions. Accepted fits are determined as those whose misfit to the mean trace element composition of a sample is lower than the critical chi-squared value. The homogenized melt compositions have a high contribution from pyroxenite-derived melts, with the highest (65 %) seen in the best fit composition to the combined Snæfellsjökull data. All flank zone melts are produced from relatively high pressures and involve low-degree melting of lherzolite (6-11 %, Figure 7).

Melting of both lherzolite and pyroxenite in the flank zone mantle are further explored in Figure 8. Model melts that match the observed flank zone compositions are produced at the greatest pressure and from the lowest degrees of melting of each lithology beneath Snæfellsjökull, and trend towards lower pressures, greater degrees of melting and greater contribution from lherzolite-derived melts from Snæfellsjökull in the West to Ytri-Rauðamelur in the East. At Surtsey, melt inclusions are best fit by homogenized melts generated at the shallower depths of melting and higher degree melts from lherzolite (11 % melting) compared to the Snæfellsnes Flank Zone.

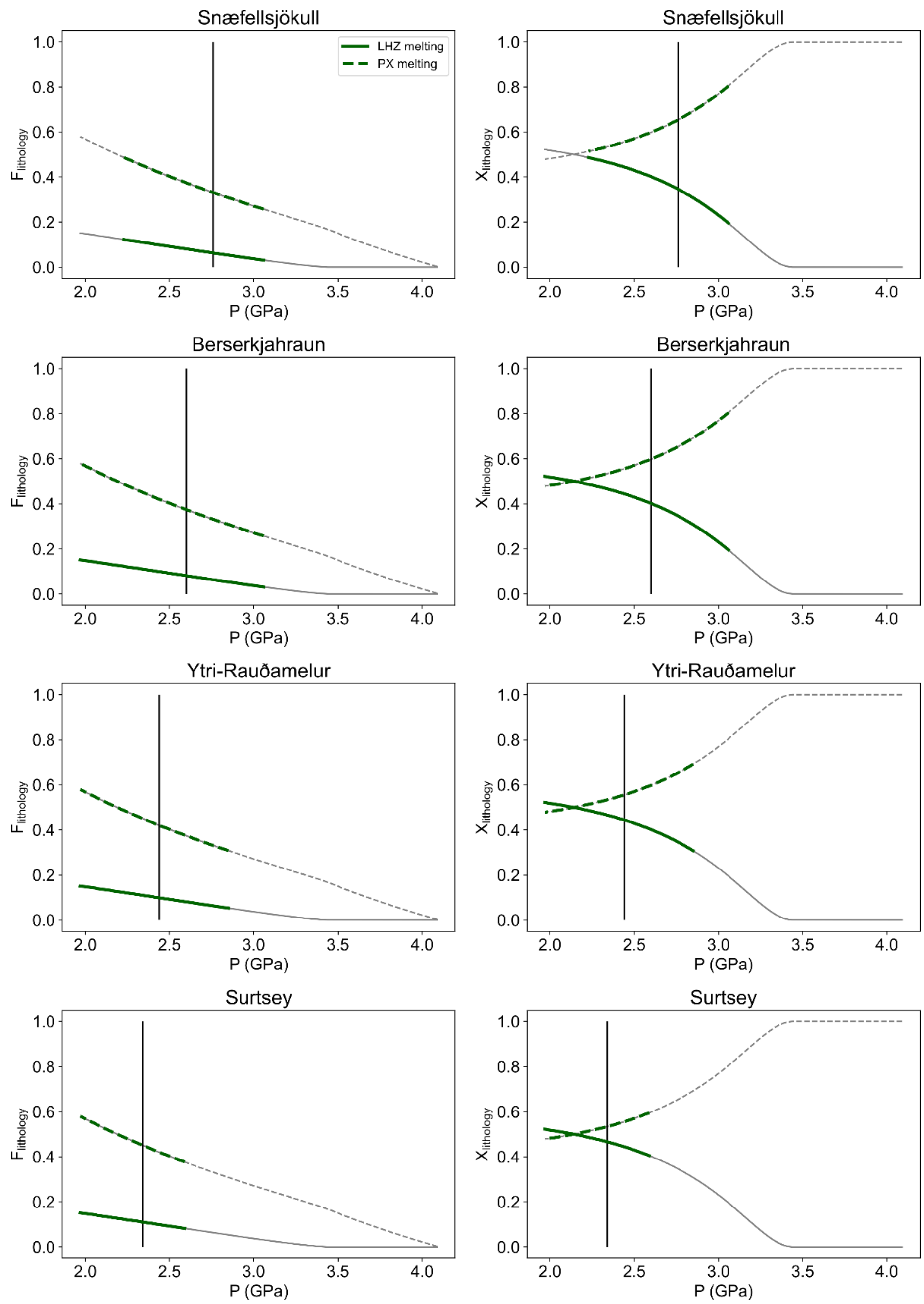

Figure 8: Lherzolite- and pyroxenite-derived melts contributing to the homogenized bulk melt composition. The grey lines show all the melting model outputs from REEBOX along the full decompression path. The green lines show the range of output melt compositions that match observed compositions below the critical chi-squared value. The best fit compositions with the lowest chi-squared value are represented by the vertical black lines. $F_{lithology}$ is the degree of fractional melting of a lithology. $X_{lithology}$ is the fraction each lithology contributes to the mixed melt composition.

3.5 Melting under Iceland's active rift zones

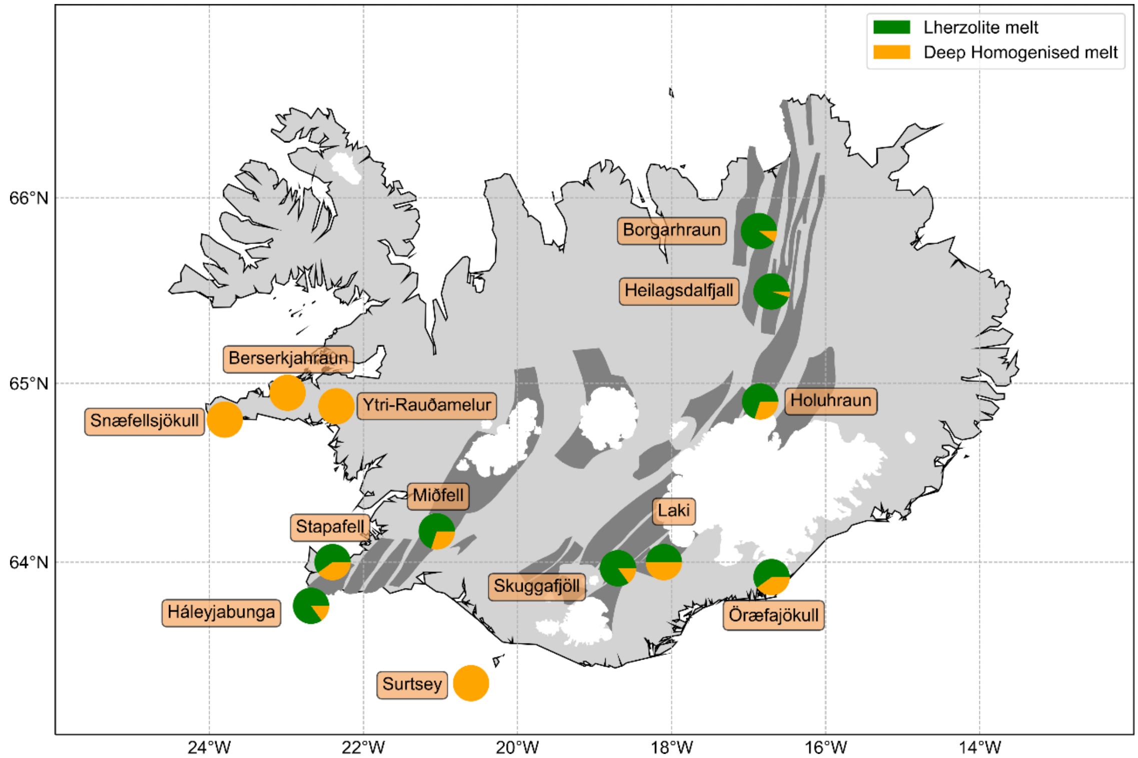

Figure 9: Map showing the contributions of deep homogenized and shallower lherzolite-derived melts to the average melt inclusion composition at different locations.

Melt inclusion compositions from the neovolcanic zone samples and Öræfajökull are modelled by mixing the deep homogenized melt composition constrained with data from Snæfellsjökull with lherzolite instantaneous melts produced at lower pressure than that of the deep homogenized melts. The contributions of the deep homogenized melts and the shallower lherzolite-derived melts that best match the observed melt inclusion compositions are summarised by Figure 9. Changing the pressure range over which shallower lherzolite instantaneous melts homogenise does not change the proportion of shallow lherzolite to deep melt that mix to produce the best fit composition presented in Figure 9. Miðfell and Háleyjabunga melt inclusions were separated into 'enriched' and 'depleted' groups due to the large variability of trace element compositions in their melt inclusion populations, and these groups were modelled separately (see supporting information). We could not determine a match for the Miðfell depleted group, even by considering only instantaneous melts of depleted lherzolite. This indicates that the mantle beneath Miðfell may include an ultra-depleted component that is not captured in our REEBOX model (cf. Gurenko and Chaussidon, 1995). Enriched Háleyjabunga melt inclusions are best fit by a 15% contribution from the deep melt component, while the depleted melt inclusions require only a 5% contribution from the deep melt component. Öraefajökull melt inclusion compositions were not matched by any of our models; the closest fit was obtained by setting the REEBOX calculation parameters to those of the EVZ (Table 2).

The misfit of the best fit compositions for each sample area is detailed in Table 2. All areas but Borgarhraun (11 elements) and Skuggafjöll (9 elements) are modelled on a 13-element system, as detailed in the methodology. For most sample areas the pressure range of lherzolite melt homogenization has negligible effect on the misfit value up to an interval of 0.5 GPa (Figure 10). A large increase in misfit in Skuggafjöll, Heilagsdalsfjall and Háleyjabunga (enriched) at the 1.5 GPa lherzolite melt homogenization range suggests that this large homogenization interval does not capture the natural processes of lherzolite melting and mixing. For Heilagsdalsfjall the lowest misfit is achieved with a homogenization range of 1 GPa and this sample may require a larger degree of homogenization of shallow lherzolite melts. Laki has the minimum misfit at low homogenization pressure range, with the misfit increasing at ranges >0.1 GPa. Borgarhraun and Háleyjabunga (depleted) show a trend towards lower misfit at larger homogenization pressure ranges. We cannot identify any spatial correlation in the degree of homogenization of lherzolite melts required to match the observed melt inclusion compositions. In the next sections we explore the model outputs for individual eruptions in each of Iceland’s active rift zones in more detail.

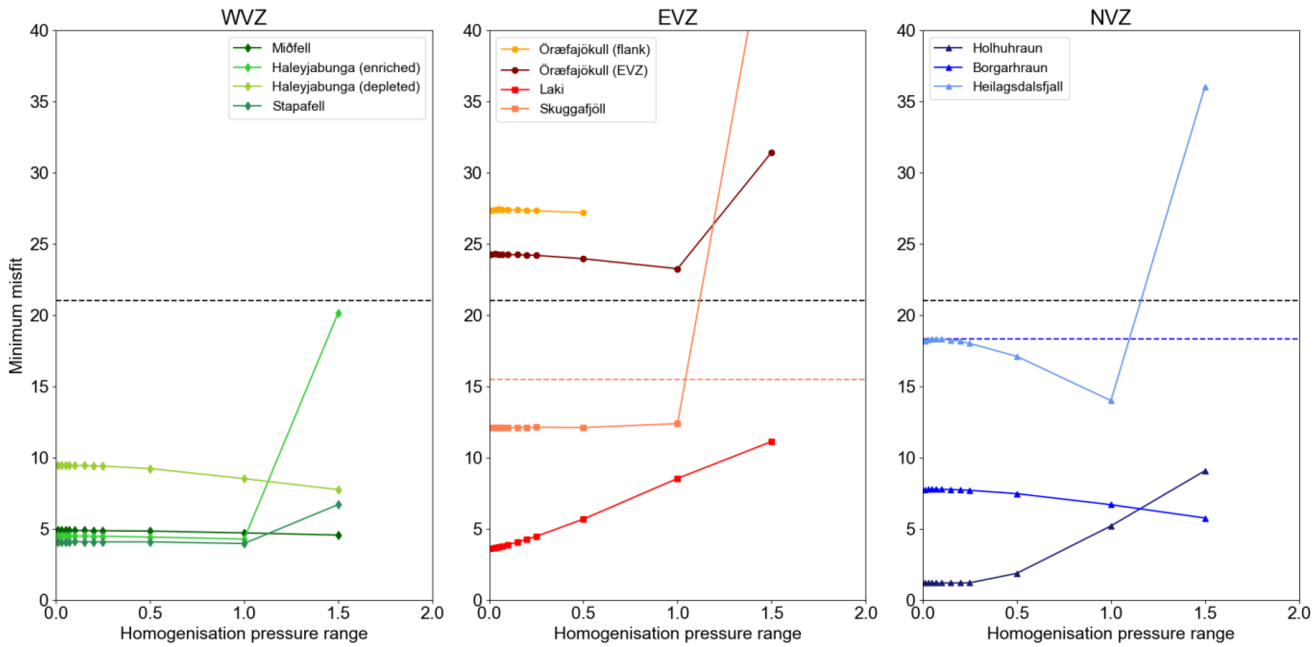

Figure 10: Minimum misfit of mixed melt compositions across differing homogenization pressure ranges. The critical chi-squared value (excluding Borgarhraun and Skuggafjöll) is shown by the black dashed line. The critical chi-squared value for Borgarhraun is shown by the blue dashed line and for Skuggafjöll by the orange dashed line.

Sample Area	Deep melt component (%)	Shallow lherzolite melt component (%)	Misfit	Homogenization pressure range (GPa)
Miðfell (enriched)	30	70	4.56	1.50
Stapafell	40	60	3.96	1.00
Háleyjabunga (enriched)	15	85	4.27	1.00
Háleyjabunga (depleted)	5	95	7.75	1.50
Laki	50	50	3.60	0.01
Skuggafjöll	15	85	12.10	0.05
Holuhraun	30	70	1.19	0.07
Borgarhraun	10	90	5.75	1.50
Heilagsdalsfjall	5	95	14.00	1.00
Öræfajökull (EVZ)	40	60	23.26	1.00
Öræfajökull (flank zone)	40	60	27.21	0.50

Table 2: Minimum misfit for each sample detailing the contributions from each lithology and homogenization intervals used.

3.6 Melting under the Western Volcanic Zone

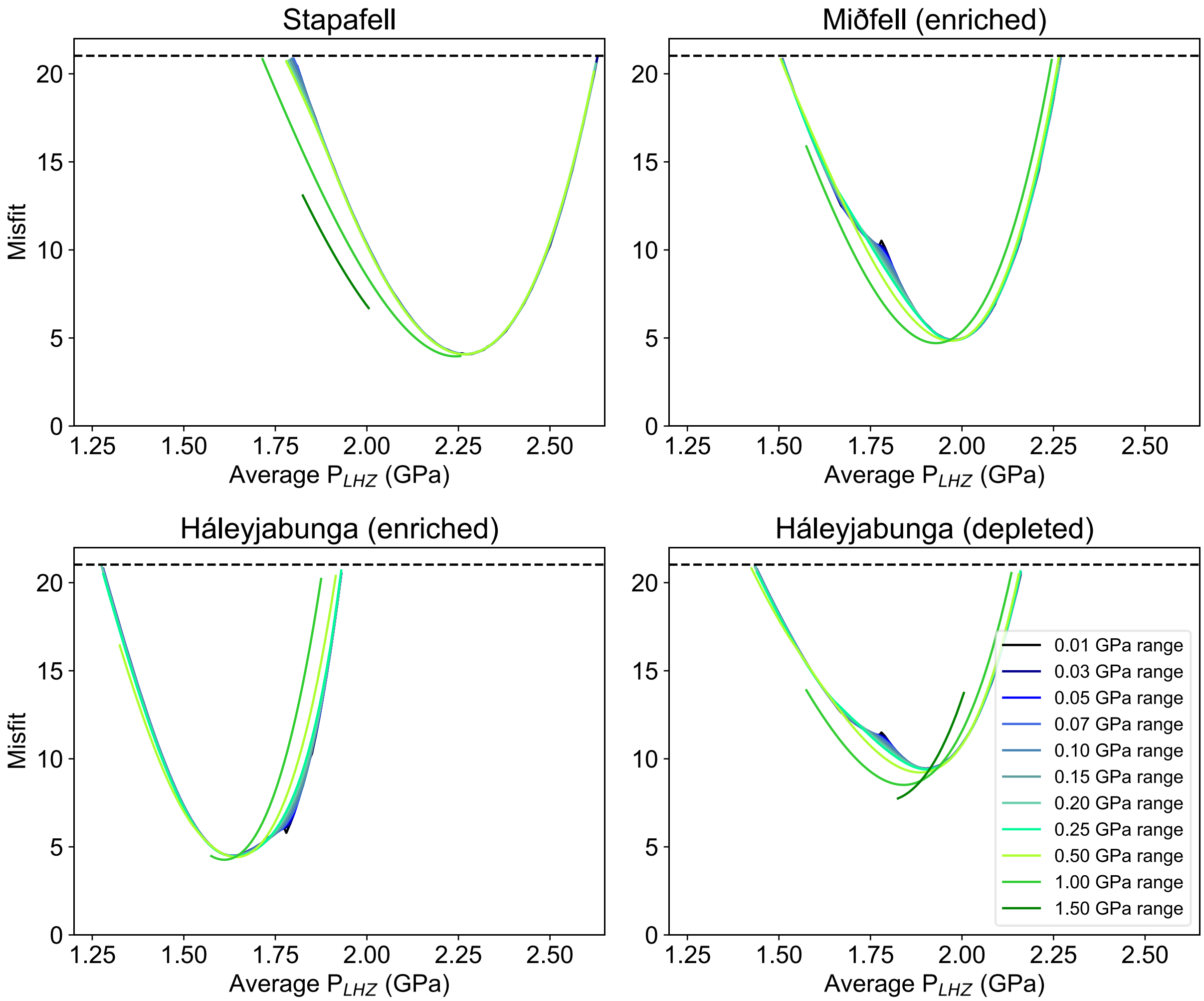

Figure 11: Average pressure of lherzolite instantaneous melt homogenization interval vs. misfit of the modelled composition to melt inclusion composition for samples in the WVZ. Critical chi-squared value = 21.03 for all sample areas shown by dashed line.

Misfits to the models of Miðfell, Háleyjabunga and Stapafell are presented in Figure 11. All homogenization pressure ranges tend to have lowest misfit at a similar mid-point of the range. That is, no matter how many melts are in the homogenized composition, the best fitting average pressure of melting in the group remains consistent. The average pressure of melting of lherzolite in the WVZ varies from ~1.6 GPa at Háleyjabunga to ~2.3 GPa at Stapafell. The average pressure of lherzolite melting in the enriched and depleted melt groupings of Háleyjabunga varies between ~1.6 GPa (enriched) and ~1.9 GPa (depleted). This, combined with the low misfit preserved at homogenization intervals of 50 and 100, suggests melts from Háleyjabunga involve homogenization of lherzolite instantaneous melts over a significant range of pressures.

3.7 Melting under the Eastern Volcanic Zone and Öræfajökull

The misfit and average pressure of melting for EVZ models are displayed in Figure 12. All sample areas show higher average pressures of melting of lherzolite than in the WVZ: from ~2.2-2.3 GPa beneath Öræfajökull and Skuggafjöll to ~2.6 GPa beneath Laki, which is just lower than the pressure the deep melt component is derived from (2.76 GPa). The lherzolite homogenization pressure range has little effect on the average pressure of melting of the lherzolite.

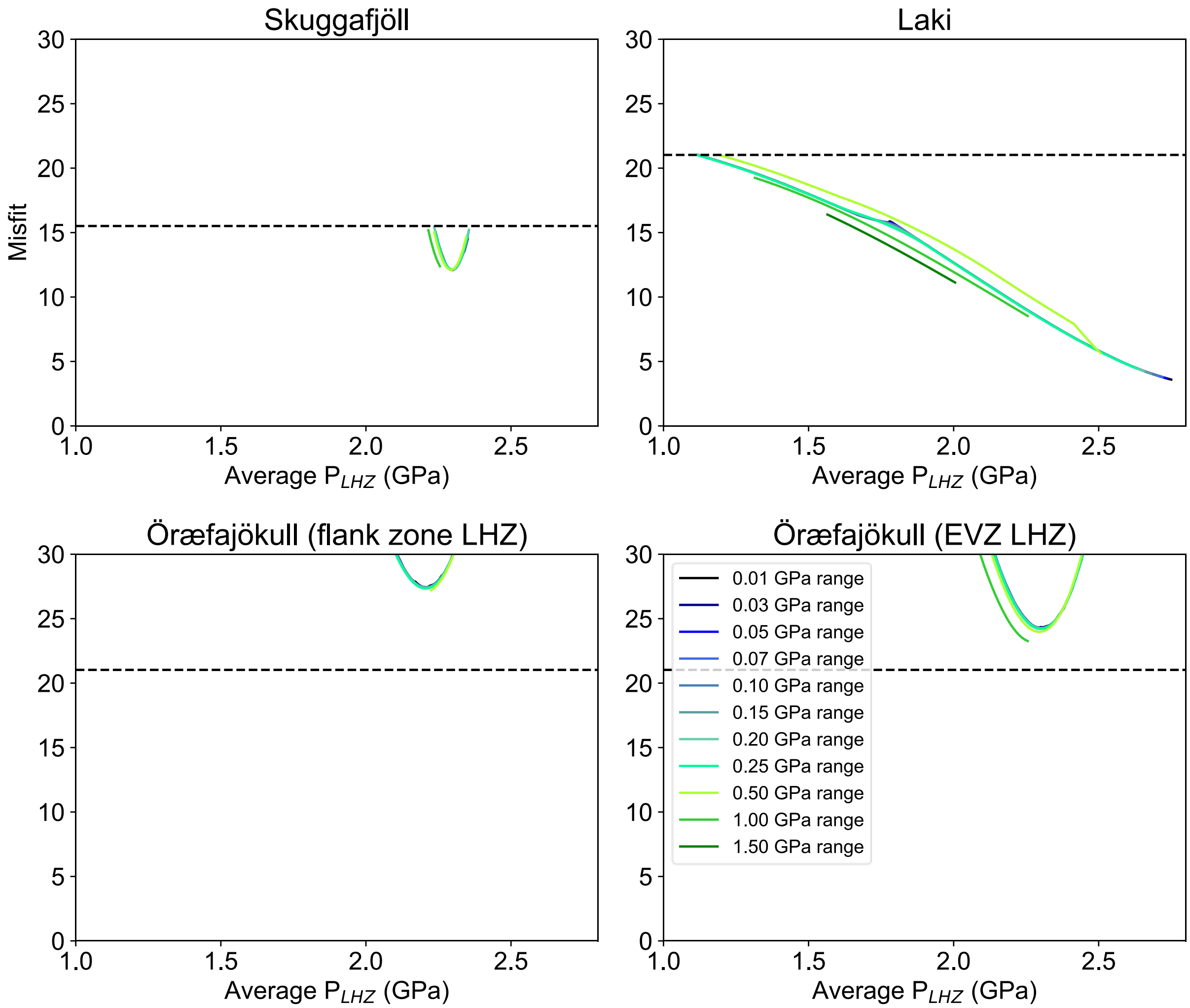

Figure 12: Average pressure of lherzolite instantaneous melt homogenization pressure range vs. misfit of the modelled composition to melt inclusion composition for samples in the EVZ. The 1.50 GPa range has been removed from Skuggafjöll as it does not return results below the critical chi-squared value. Critical chi-squared values are shown by dashed lines: 21.03 for Laki and Öræfajökull, and 15.51 for Skuggafjöll.

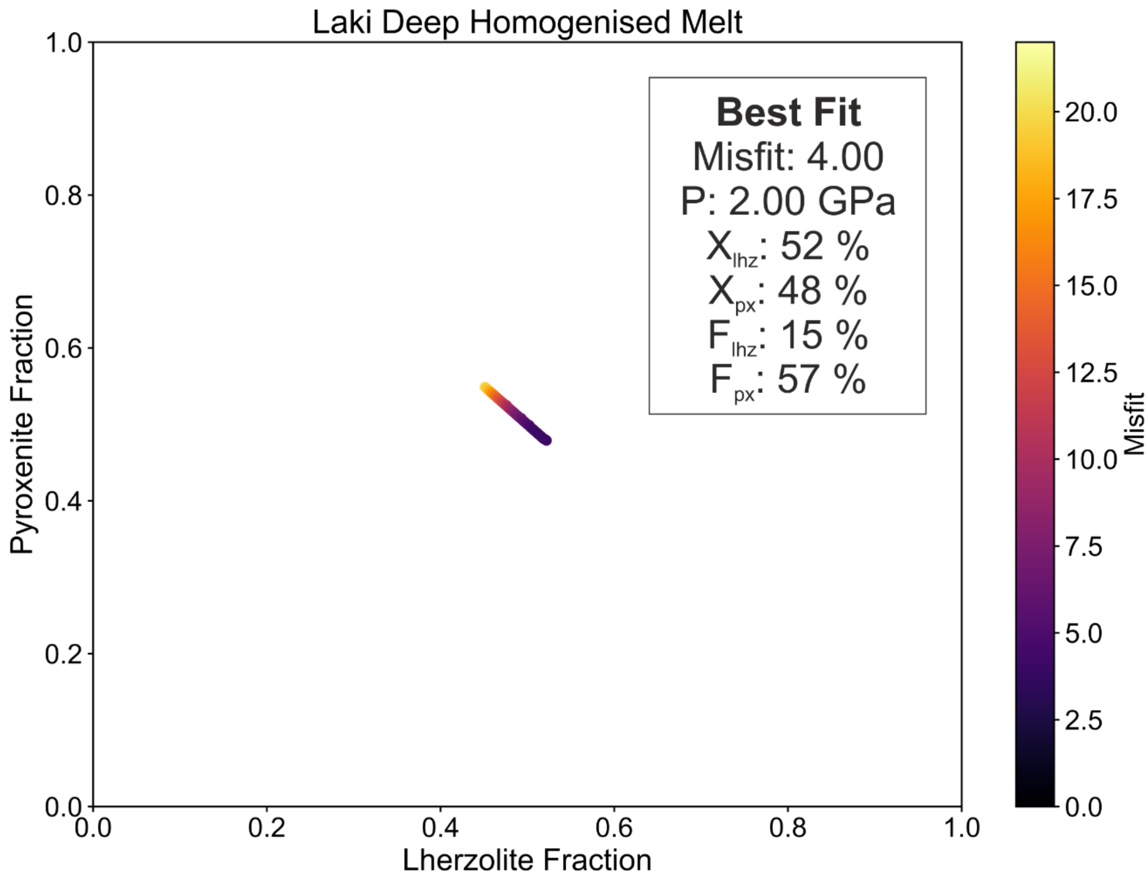

Figure 13: Misfit of the deep homogenized composition modelled beneath the flank zones in REEBOX compared to the mean melt inclusion composition of Laki. Fractions on axes refer to the fraction of melts from each lithology in the homogenized melts. Results below the critical chi-squared value are returned for Laki using both the deep homogenized melt and mixing the homogenized melt with shallower lherzolite-derived melts. F refers to the melt fraction of each lithology. X refers to the contribution of melts from each lithology to the homogenized melts. Px = pyroxenite, lhz = lherzolite.

Laki has anomalous results compared to the other locations as the average pressure does not converge on a minimum as an inverted bell curve (Figure 12). Instead, the minimum misfit is achieved by mixing lherzolite instantaneous melts produced just after the homogenization of the deep melt component (Figure 12). The deep homogenized column-accumulate melts produced by REEBOX for the flank zones can also provide a match to the composition of Laki melt inclusions if more than 5% melting of lherzolite is allowed to occur before homogenization. The best fit (deep) homogenized composition is detailed in Figure 13. This melt involves 15%

fractional melting of lherzolite before homogenization, with melting occurring at ~2.0 GPa. This melt also requires greater input of lherzolite-derived melts compared to the composition derived for the flank zones.

3.8 Melting under the Northern Volcanic Zone

Figure 14 details the average pressure of lherzolite melt homogenization, and the corresponding misfits, for samples in the NVZ. The average pressure only varies on reaching high homogenization pressure range (1.0-1.5 GPa). All areas require melting of lherzolite at pressures similar to the EVZ. Shallower lherzolite-derived melts are drawn from lower pressures at Borgarhraun (~2.1-2.2 GPa) compared to Heilagsdalsfjall and Holuhraun (>2.3 GPa).

Holuhraun shows an anomalous trend similar to that of Laki (Figure 14). When the melt inclusion compositions of Holuhraun are compared to the deep melt generated in the flank zones, no match is found to the measured compositions.

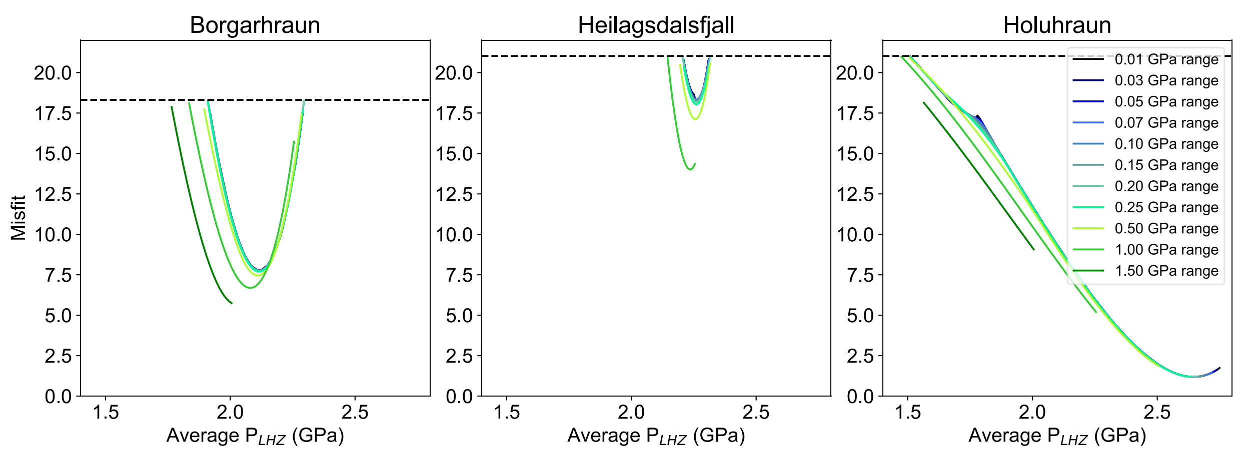

Figure 14: Average pressure of lherzolite instantaneous melt homogenization interval vs. misfit of the modelled composition to melt inclusion composition for samples in the NVZ. The 1.5 GPa homogenization range has been removed from Heilagsdalsfjall as it does not return results below the critical chi-squared value. Critical chi-squared values are 21.03 for Heilagsdalsfjall and Holuhraun, and 18.31 for Borgarhraun.

4 Discussion

4.1 Variation in the depth of melt homogenization across Iceland

As seen in Figure 7 (section 3.4) a single composition of deep homogenized melts modelled beneath the flank zones does not provide the best fit to all the flank zone data. In each of the flank zones the pressure at which melts homogenise, the degrees of melting of each lithology and proportional input from each lithology vary. The melt composition determined from Snæfellsjökull provides the closest match to the model envisaged by Rudge et al. (2013), where homogenization occurs with lherzolite-derived melts produced before ~5 % melting of lherzolite. Moving east along the Snæfellsnes Flank Zone to Berserkjahraun and Ytri-Rauðamelur, the deep homogenized melt requires mixing with melts derived from higher degrees of melting from both lherzolite and pyroxenite at lower pressures than that observed in Snæfellsjökull. This is also true of Surtsey, where lherzolite is predicted to undergo 11 % melting before homogenization of the melts. The variation in pressure where the deep melt is produced beneath the flank zones shown in Figure 8.

Hardarson and Fitton (1991) demonstrated that differences in trace element compositions of basalts from Snæfellsjökull result from glacial retreat and isostatic rebound increasing the degree of mantle melting and shifting from the garnet stability field to the spinel stability field. The increase in the degree of melting of lithologies in the mantle beneath the Snæfellsnes Flank Zone could be influenced by changing ice thickness altering the melting behaviour of the mantle. However, the variation of melting in Surtsey cannot be linked to the same rebound in the SFZ, as it is spatially distant and postdates ice-sheet retreat.

The homogenized compositions of deep melts expressed in flank zone melt inclusions reflect the onset of channelization in the mantle (Rudge et al., 2013). Channelization results in rapid transport of partial mantle melts to the surface, preserving heterogenous melt compositions (Spiegelman and Katz, 2003; Weatherly and Katz, 2012). The models of the homogenized deep melt from the flank zones in this study suggest that the threshold for onset of channelization may be somewhat variable across Iceland.

Öræfajökull is an anomalous flank zone system as it appears to require a contribution from shallower lherzolite-derived melt in addition to the deep homogenized melt. This could be influenced by the ridge jump towards Eastern Iceland that is transferring rift-type melting towards the Snæfell-Öræfajökull Flank Zone (Einarsson, 2008). This may explain the better fit of the Öræfajökull model using shallow lherzolite melts from the EVZ melting regime. Additionally, thinner lithosphere beneath Öræfajökull compared to Snæfellsjökull would mean lherzolite melts may be derived at shallower mantle depths compared to other flank zones. There are only six measured melt inclusion compositions from Öræfajökull. Greater sampling may provide a more accurate mean melt composition for the model to match. Recycled sediment is thought to contribute to the melt composition at Öræfajökull (Prestvik et al., 2001; Kokfelt et al., 2006; Manning and Thirlwall, 2014), but this is not accounted for in our model and could explain the poor fits.

The model shows two possibilities for the generation of Laki melt inclusion compositions. The first scenario allows greater flexibility in the generation of the deep homogenized melt composition across Iceland, whereby higher degrees of lherzolite melting can occur before the deep melt component is homogenized. The second scenario requires restricting the range of melting that produces the deep homogenized melt to a limited pressure across Iceland and mixing with deeper lherzolite instantaneous melts shortly after homogenization.

Holuhraun shows a similar trend to Laki however there is no match found between Holuhraun melt inclusions and the homogenized composition when produced at lower pressure and with greater degrees of melting of lherzolite than in the flank zones. This suggests that, for Holuhraun, it is more likely that a deep homogenized component similar to that produced at Snæfellsjökull, mixes with lherzolite instantaneous melts formed at pressures just above where the homogenized melt is produced. As Laki and Holuhraun are both located in central Iceland, melting of lherzolite at higher pressures could be linked to their proximity to the plume centre.

4.2 Variation in the depth of shallow lherzolite-derived melt across Iceland

Mixing of deep homogenized melts with shallower lherzolite-derived melts is an important mechanism for generating variable melt compositions in the axial rift zones. Figure 15 shows the average pressures at which lherzolite melts are sourced in each sample area to mix with the deep melt component and provide the best fit to sample data. Shallower lherzolite-derived melts appear to be sourced at the greatest pressure in central Iceland, close to the proposed plume centre. This pressure decreases northwards along the NVZ and the lowest pressures of melting are observed in the WVZ. The pressures of lherzolite melting in central Iceland are close to the pressure where the deep homogenized component is derived. This suggests that mixing of the homogenized melt and lherzolite-derived melts happens at greater depths in the mantle with greater proximity to the mantle plume centre. The higher pressure of melting and lower melt fractions involved in central Iceland (Holuhraun and Laki) correlate with crustal thickness (Jenkins et al., 2018). A thicker lithospheric lid has been shown generate lower melt fractions in central Iceland compared to elsewhere along axial rifts (Harðardóttir et al., 2022). Deeper melting in central Iceland is therefore likely also partly a consequence of the thicker crust, with decreasing crustal thickness in the volcanic zones allowing for higher melt fractions to be generated.

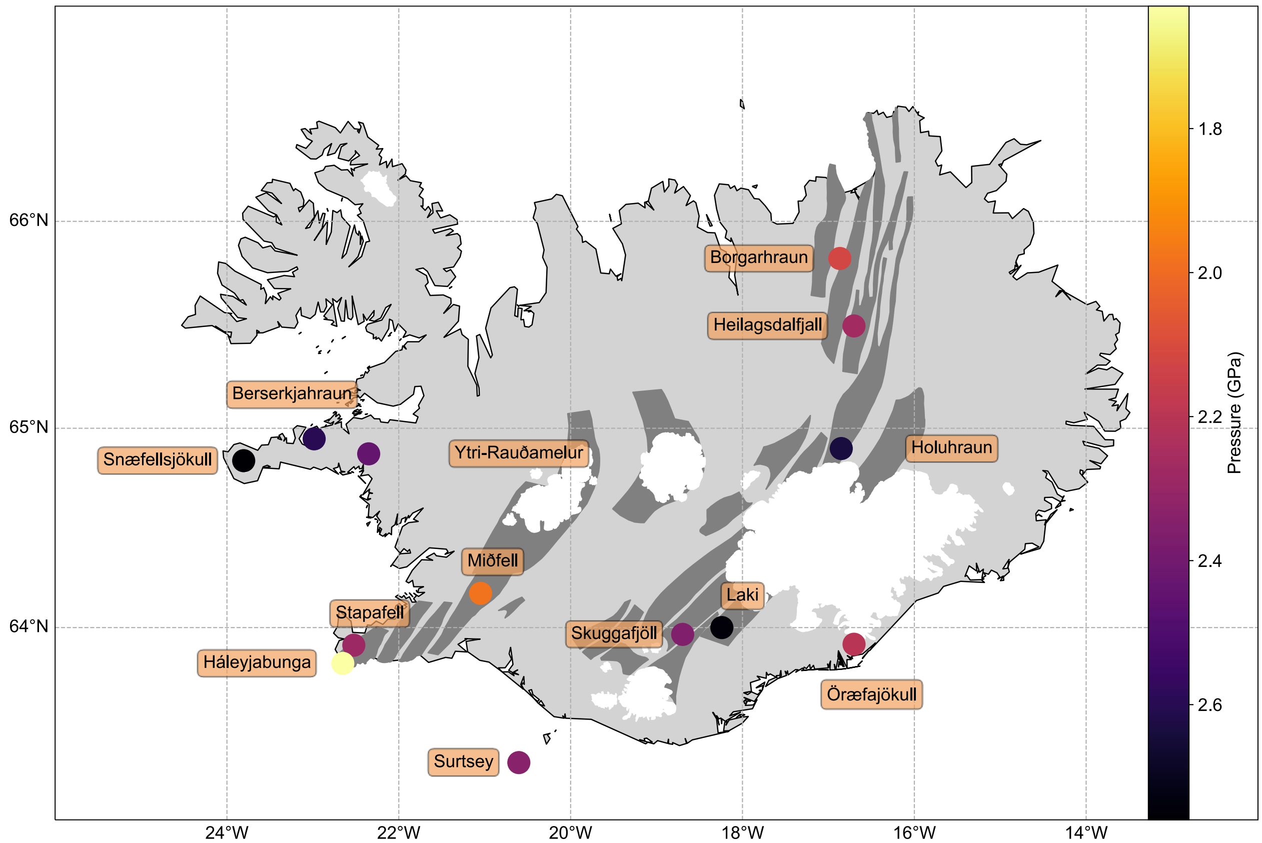

Figure 15: Average pressure of melting of lherzolite melt (using the 0.03 GPa homogenization range) which provides the best fit model composition for each sample area (neovolcanic zones and Öræfajökull (flank zone melt regime). Flank zones show best fit pressure of melting for deep homogenized melt.

The source of lherzolite melts close to the pressure where the deep melt component is generated at both Laki and Holuhraun raises further questions about how this deep melt component is produced and when channelization begins across the Icelandic mantle. Allowing homogenization to take place at shallower depths (i.e., lower pressure and greater degrees of melting) can explain the compositions of melt inclusions from Laki, but not Holuhraun. The observations from Laki may be consistent with a propagating rift and a mantle less preconditioned to host channels, resulting in later onset of channelization. Although more extensive melting and homogenization prior to channelization may occur near the plume centre, our homogenized melt component alone cannot match all the compositions observed in central Iceland. Further mixing with shallower lherzolite-derived melts following the onset of channelization may still be required for some areas of central Iceland, such as Holuhraun. Denser coverage of melt inclusion studies across both central Iceland and the neovolcanic zones would allow us to determine if the proposed changes in melting and homogenization of mantle melts is true of all locations near the plume centre, or a localised feature that is distinctive of Laki and Holuhraun.

To convert our proposed best fit pressures to depths where melting occurs for either the deep homogenized melt or shallower lherzolite melts, we employ the hydrostatic equation to calculate a suitable relative depth in the mantle. We separate the overlying crustal thicknesses from the unknown depth of mantle as follows:

$$\boldsymbol{P = \rho_1 g h_1 + \rho_2 g h_2}$$

Where P = pressure (GPa), g = acceleration due to gravity (9.8 ms^{-1}), ρ_1 = density of crust (kg/m^3), ρ_2 = density of mantle (kg/m^3), h_1 = thickness of crust (km), h_2 = thickness of mantle (km). Densities and crustal thicknesses were taken from Staples et al. (1997) and Bjarnason and Schilling (2009) respectively (Table 1). Taking the pressure of melting determined for a harzburgite-bearing mantle, we calculated depths of melting for lherzolite and pyroxenite in each sample area (Table 3).

Sample Area	**Melt component**	**Best fit pressure (GPa)**	**Calculated depth (km)**
Snæfellsjökull	Deep homogenized melt	2.76	93
Ytri-Rauðamelur	Deep homogenized melt	2.44	83
Berserkjahraun	Deep homogenized melt	2.60	88
Surtsey	Deep homogenized melt	2.34	80
Stapafell	Shallower lherzolite	2.28	78
Háleyjabunga (enriched)	Shallower lherzolite	1.63	57
Háleyjabunga (depleted)	Shallower lherzolite	1.90	66
Miðfell (enriched)	Shallower lherzolite	1.98	68
Laki	Shallower lherzolite	2.74	93
Skuggafjöll	Shallower lherzolite	2.29	79
Holuhraun	Shallower lherzolite	2.64	90
Heilagsdalsfjall	Shallower lherzolite	2.27	78
Borgarhraun	Shallower lherzolite	2.12	73
Öræfajökull (flank zone)	Shallower lherzolite	2.20	76
Öræfajökull (EVZ)	Shallower lherzolite	2.30	79

Table 3**:** Depths where shallow lherzolite-derived melts (neovolcanic zones) or the homogenized deep melt component (flank zones) are produced, determined for each sample area. The pressure used to calculate melting of shallow lherzolite is from the 0.03 GPa homogenization range.

4.3 Varying the melting model inputs: lithological proportions and temperature

Our model makes several assumptions to look at variations across Iceland. Firstly, we have assumed that the proportions of lherzolite, pyroxenite and harzburgite in the mantle remain constant across all of Iceland. This decision was made to simplify the model and only consider variations caused by differing input of melts derived from different lithologies. Further work to determine how proportions of mantle lithologies vary across the flank and neovolcanic zone on a smaller scale would be beneficial before attempting our modelling technique with different lithological proportions.

We investigated two scenarios for Snæfellsjökull with different lithological proportions in the mantle from our initial model, greater pyroxenite and greater harzburgite, to see what effect this had on the genesis of deep homogenized melts. Increasing the percentage of pyroxenite in the mantle from 10% to 15% (55% lherzolite: 15% pyroxenite: 30% harzburgite) resulted in the best fit melt composition being produced at a lower pressure (2.56 GPa compared to 2.76 GPa) and a greater input from pyroxenite-derived melts (72% compared to 65%). Both lherzolite and pyroxenite underwent similar degrees of melting in the higher pyroxenite model. Increasing the proportion of harzburgite in the mantle to 45% (with the same 10% KG1 pyroxenite; 45% lherzolite: 10% pyroxenite: 45% harzburgite) resulted in the best fit melt being produced at a similar pressure and from similar degree of melting but increased the contribution of pyroxenite-derived melt in the homogenized melt (70%). These results show that changing the proportion of pyroxenite and lherzolite in the mantle across Iceland determines the proportion of melts from each lithology that contributes to the deep homogenized component, similar to the findings of Shorttle et al. (2014). Lithological differences may also affect the pressure at which melts are produced, even though the degree of melting that each lithology undergoes is relatively unchanged.

We assumed a constant mantle potential temperature of 1480°C (Matthews et al., 2016) to model all our sample areas. While this removes a variable from our modelling, there will be some natural variation in the mantle potential temperature across Iceland. Harðardóttir et al. (2022) suggest that mantle potential temperature has only a limited effect on melt fraction and the generation of geochemical heterogeneity, and that melting in off-axis flanks zones occurs within the same temperature range as the axial rift zones (1299-1539 °C). Nonetheless, we investigated the extreme case where there is no temperature anomaly beneath the Snæfellsnes Flank Zone, assuming an ambient mantle potential temperature of 1318 °C (Matthews et al., 2016), and an intermediate case with a nominal T_p of 1390 °C. At T_p of 1318°C no aggregate melt composition could match the measured melt inclusion compositions. At 1390 °C the best fit homogenized melt composition has a misfit of 5.55 and is produced at 1.96 GPa and comprises 27% lherzolite-derived melts and 73% pyroxenite-derived melts. For comparison, the best fit melt composition produced with a T_p of 1480 °C has a misfit of 7.21 and is produced at 2.76 GPa, with 35% lherzolite-derived melts and 65% pyroxenite-derived melts. The fraction of melting changes slightly with 4% melting of lherzolite instead of 6%. A thermal anomaly is therefore required beneath the Snæfellsnes Flank Zone, but if the thermal anomaly is lower than that under central Iceland then melting would necessarily take place at shallower depths and a higher contribution from pyroxenite-derived melts to the homogenized melt is required.

Neave et al. (2019) showed that in magmatic systems with geochemically variable input melts, enriched melt compositions survive crustal processing more effectively than depleted compositions, which biases erupted compositions towards those from enriched recycled lithologies. As the majority of melt inclusion compositions measured and used in this study are primitive, they are relatively robust to modification during crystallisation and processing in the crust. This is true whether modification concerns mixing biasing towards enriched compositions (Neave et al., 2019) or modification by the RTMX processes (O'Neill and Jenner, 2012).

4.4 Pyroxenite in the Icelandic Mantle

Our study shows that pyroxenite lithologies are present in both the rift and flank zones of the Icelandic mantle, as well as near to and far from the plume centre. Pyroxenite-derived melts contribute to deep homogenized melts when mixed with low-degree lherzolite melts. These homogenized melts then mix with lherzolite melts produced at shallower depths in the mantle to produce the trace element compositions observed in the neovolcanic zones.

Rasmussen et al. (2020) argue that olivine compositions from the Snæfellsnes Flank Zone show that melts are derived from a purely peridotitic mantle, with no contribution from a recycled pyroxenite lithology. They specifically refer to the Snæfellsnes source being olivine-bearing, and suggest that enriched compositions may be linked to a refertilised peridotite source. The KG1 pyroxenite of Kogiso et al. (1998) used in our model is a silica-deficient olivine-bearing lithology generated by mixing 50% MORB with 50% KLB-1 peridotite. Thus, our model does not require that recycled oceanic lithosphere is a distinct olivine-free pyroxenite in the Icelandic mantle. Rather, we suggest that the recycled material has mixed with surrounding peridotite to create a modally enriched, olivine-bearing pyroxenite-lherzolite hybrid lithology. Modally enriched components in the mantle may be enriched in pyroxene (±garnet) whilst also containing olivine, as has been inferred for the Icelandic mantle by Shorttle and Maclennan (2011); Neave et al. (2018) likewise conclude that enriched heterogeneities in the Icelandic mantle are olivine-bearing lithologies. Lambart et al. (2017) modelled decompression melting of G2 (eclogite), KG1 (50% MORB + 50% peridotite) and KG2 (33% MORB + 66% peridotite) in the Icelandic mantle under a potential temperature of 1480 °C (as used in this study). In this model, the trace elements and isotopic systems of Icelandic basalts are best fit by a mantle containing 20% KG1, indicating that recycled material refertilises peridotites in the Icelandic mantle to create a hybrid lithology. We therefore agree with Rasmussen et al. (2020) that the enriched lithology present in the Icelandic mantle must be a hybrid pyroxenite-peridotite composition such as KG1, and not unreacted olivine-free pyroxenites. Modally enriched peridotites generated from the refertilisation of peridotite with recycled crustal material (e.g. Yaxley and Green., 1998) may be important lithologies in the widespread production of oceanic melts (Neave et al., 2018).

5 Conclusions

Collection of new melt inclusion compositions and models of mantle melting beneath Iceland's flank zones show that the trace element compositions of samples in the SFZ and Surtsey can be generated by deep homogenized melts similar to those envisaged by Rudge et al. (2013). These homogenized components are the result of mixing low-degree melts of lherzolite with higher-degree melts of pyroxenite produced at ~2.35-2.75 GPa. The Rudge et al. (2013) model suggests homogenzsed melts include lherzolite-derived melts produced at up to 5% lherzolite melting.

Our models suggest that the lherzolite melt fraction could be as high as 15% for samples in the SNF.

The neovolcanic zones and Öræfajökull require the deep homogenized melt to mix with lherzolite instantaneous melts produced at lower pressures, following onset of channelization, to match measured melt inclusion compositions. The pressure these instantaneous melts are sampled at varies with locality, but we observe an increase in pressure (and therefore depth in the mantle) in samples closer to the mantle plume centre. The proportion of the deep homogenized melt contributing to the modelled melt composition is greatest close to the plume centre and is markedly lower in the NVZ than elsewhere in Iceland. The NVZ has previously shown to be geochemically distinct from Iceland, particularly in lithophile isotopic composition. Laki also provides evidence that at localities closer to the mantle plume homogenization of lherzolite- and pyroxenite-derived melts occurs shallower depths in the mantle prior to the onset of channelisation. Further work is required to constrain how the production of the deep homogenized melt varies across Iceland, and whether a homogenized component is of greater influence closer to the plume centre than elsewhere in the neovolcanic zones.

Our results are consistent with previous suggestions that Phanerozoic-age subducted lithosphere, possibly associated with Iapetus closure, is present in the upper mantle of the North Atlantic (Thirlwall et al., 2004; McKenzie et al., 2004; Halldórsson et al., 2016b). The rising Icelandic mantle plume then entrains this recycled material as it rises through the upper mantle. Low-degree melting beneath the Snæfellsnes Flank Zone and Surtsey, far from the centre of the mantle plume, results in bulk melt compositions being dominated by melts source from the ITE-enriched recycled material relative to surrounding lherzolite, producing highly ITE-enriched compositions of the flank zone basalts.

Acknowledgments

The authors thank Dr Jonathan Fellowes and Dr Stuart Kearns for their assistance with EPMA analysis and Dr Cristina Talavera and Dr John Craven for assistance with SIMS analysis. We thank Dr Alison Pawley for constructive comments on an early draft of this manuscript. This work was funded through a NERC studentship to Waters through the Manchester-Liverpool

Doctoral Training Partnership NE/L002469/1, NERC grant NE/P002331/1 and IMF grant 638/1017.

Open Research

Composition data of measured melt inclusions and crystal hosts are available as an excel spreadsheet from https://doi.org/10.48420/21688895.v1. Additional figures and detailed explanations of the post entrapment crystallization corrections carried out in this work are included in the supplementary material. The code developed for the modelling in this work is available from https://github.com/emmacwaters/meltmix.

References

Beattie, P. (1994). Systematics and energetics of trace-element partitioning between olivine and silicate melts: Implications for the nature of mineral/melt partitioning. *Chemical Geology*, *117*(1), 57–71. https://doi.org/https://doi.org/10.1016/0009-2541(94)90121-X

Bjarnason, I. T., & Schmeling, H. (2009). The lithosphere and asthenosphere of the Iceland hotspot from surface waves. *Geophysical Journal International*, *178*(1), 394–418. https://doi.org/10.1111/j.1365-246X.2009.04155.x

Brown, E. L., Petersen, K. D., & Lesher, C. E. (2020). Markov chain Monte Carlo inversion of mantle temperature and source composition, with application to Reykjanes Peninsula, Iceland. *Earth and Planetary Science Letters*, *532*, 116007. https://doi.org/10.1016/j.epsl.2019.116007

Brown, E. L., & Lesher, C. E. (2016). REEBOX PRO: A forward model simulating melting of thermally and lithologically variable upwelling mantle. *Geochemistry, Geophysics, Geosystems*, *17*(10), 3929–3968. https://doi.org/10.1002/2016GC006579

Chauvel, C., & Hémond, C. (2000). Melting of a complete section of recycled oceanic crust: Trace element and Pb isotopic evidence from Iceland. *Geochemistry, Geophysics, Geosystems*, *1(2)*, 1–22. https://doi.org/10.1029/1999GC000002

Danyushevsky, L. V., & Plechov, P. (2011). Petrolog3: Integrated software for modeling crystallization processes. *Geochemistry, Geophysics, Geosystems*, *12(7), Q07021*. https://doi.org/10.1029/2011GC003516

Darbyshire, F. A., Bjarnason, I. T., White, R. S., & Flóvenz, Ó. G. (1998). Crustal structure above the Iceland mantle plume imaged by the ICEMELT refraction profile. *Geophysical Journal International*, *135*(3), 1131–1149. https://doi.org/10.1046/j.1365-246X.1998.00701.x

Darbyshire, F. A., Priestley, K. F., White, R. S., Stefánsson, R., Gudmundsson, G. B., & Jakobsdóttir, S. S. (2000b). Crustal structure of central and northern Iceland from analysis of teleseismic receiver functions. *Geophysical Journal International*, *143(1)*, 163-184. https://doi.org/10.1046/j.1365-246X.2000.00224.x

Darbyshire, F. A., White, R. S., & Priestley, K. F. (2000a). Structure of the crust and uppermost mantle of Iceland from a combined seismic and gravity study. *Earth and Planetary Science Letters*, *181(3)*, 409-428. https://doi.org/10.1016/S0012-821X(00)00206-5

Einarsson, P. (2008). Plate boundaries, rifts and transforms in Iceland. *Jokull*, *58*(58), 35–58.

Fitton, J. G., Saunders, A. D., Kempton, P. D., & Hardarson, B. S. (2003). Does depleted mantle form an intrinsic part of the Iceland plume? *Geochemistry, Geophysics, Geosystems*, *4*(3), 1–14. https://doi.org/10.1029/2002GC000424

Fitton, J. G., Saunders, A. D., Norry, M. J., Hardarson, B. S., & Taylor, R. N. (1997). Thermal and chemical structure of the Iceland plume. *Earth and Planetary Science Letters*, *153*(3–4), 197–208. https://doi.org/10.1016/S0012-821X(97)00170-2

Gurenko, A. A., & Chaussidon, M. (1995). Enriched and depleted primitive melts included in olivine from Icelandic tholeiites: origin by continuous melting of a single mantle column. *Geochimica et Cosmochimica Acta*, *59*(14), 2905–2917. https://doi.org/10.1016/0016-7037(95)00184-0

Gurenko, A. A., & Sobolev, A. V. (2006). Crust-primitive magma interaction beneath neovolcanic rift zone of Iceland recorded in gabbro xenoliths from Midfell, SW Iceland. *Contributions to Mineralogy and Petrology*, *151*(5), 495–520. https://doi.org/10.1007/s00410-006-0079-2

Halldórsson, S. A., Barnes, J. D., Stefánsson, A., Hilton, D. R., Hauri, E. H., & Marshall, E. W. (2016a). Subducted lithosphere controls halogen enrichments in the Iceland mantle plume source. *Geology*, *44*(8), 679–682. https://doi.org/10.1130/G37924.1

Halldórsson, S. A., Hilton, D. R., Barry, P. H., Füri, E., & Grönvold, K. (2016b). Recycling of crustal material by the Iceland mantle plume: New evidence from nitrogen elemental and isotope systematics of subglacial basalts. *Geochimica et Cosmochimica Acta*. https://doi.org/10.1016/j.gca.2015.12.021

Hanan, B. B., Blichert-Toft, J., Kingsley, R., & Schilling, J.-G. (2000). Depleted Iceland mantle plume geochemical signature: Artifact of multicomponent mixing? *Geochemistry, Geophysics, Geosystems*, *1*(4). https://doi.org/https://doi.org/10.1029/1999GC000009

Harðardóttir, S., Halldórsson, S. A., & Hilton, D. R. (2018). Spatial distribution of helium isotopes in Icelandic geothermal fluids and volcanic materials with implications for location, upwelling and evolution of the Icelandic mantle plume. *Chemical Geology*, *480*, 12–27. https://doi.org/10.1016/j.chemgeo.2017.05.012

Harðardóttir, S., Matthews, S., Halldórsson, S. A., Jackson, M. G. (2022). Spatial distribution and characterization of Icelandic melt end-members: Implications for plume geometry and melting processes. *Chemical Geology*, 604, 120930. https://doi.org/10.1016/j.chemgeo.2022.120930

Hardarson, B. S., & Fitton, J. G. (1991). Increased mantle melting beneath Snaefellsjökull volcano during Late Pleistocene deglaciation. *Nature*, *353*(6339), 62–64. https://doi.org/10.1038/353062a0

Hartley, M. E., Bali, E., Maclennan, J., Neave, D. A., & Halldórsson, S. A. (2018). Melt inclusion constraints on petrogenesis of the 2014–2015 Holuhraun eruption, Iceland. *Contributions to Mineralogy and Petrology*, *173*(2), 10. https://doi.org/10.1007/s00410-017-1435-0

Harrison, D., Burnard, P., & Turner, G. (1999). Noble gas behaviour and composition in the mantle: Constraints from the Iceland plume. *Earth and Planetary Science Letters*, *171*(2), 199–207. https://doi.org/10.1016/S0012-821X(99)00143-0

Hauri, E. H., Maclennan, J., McKenzie, D., Gronvold, K., Oskarsson, N., & Shimizu, N. (2018). CO2 content beneath northern Iceland and the variability of mantle carbon. *Geology*, *46*(1), 55–58. https://doi.org/10.1130/G39413.1

Hémond, C., Arndt, N. T., Lichtenstein, U., Hofmann, A. W., Oskarsson, N., & Steinthorsson, S. (1993). The heterogeneous Iceland plume: Nd-Sr-O isotopes and trace element constraints. *Journal of Geophysical Research*, *98*(B9), 15833. https://doi.org/10.1029/93JB01093

Hirschmann, M. M., Kogiso, T., Baker, M. B., & Stolper, E. M. (2003). Alkalic magmas generated by partial melting of garnet pyroxenite. *Geology*, *31*(6), 481–484. https://doi.org/10.1130/0091-7613(2003)031<0481:AMGBPM>2.0.CO;2

Hofmann, A. W., & White, W. M. (1982). Mantle plumes from ancient oceanic crust. *Earth and Planetary Science Letters*, *57*(2), 421–436. https://doi.org/10.1016/0012-821X(82)90161-3

Jarosewich, E., Nelen, J. A., & Norberg, J. A. (1980). Reference Samples for Electron Microprobe Analysis. *Geostandards Newsletter*, *4*(1), 43–47. https://doi.org/https://doi.org/10.1111/j.1751-908X.1980.tb00273.x

Jenkins, J., Maclennan, J., Green, R. G., Cottaar, S., Deuss, A. F., & White, R. S. (2018). Crustal Formation on a Spreading Ridge Above a Mantle Plume: Receiver Function Imaging of the Icelandic Crust. *Journal of Geophysical Research: Solid Earth*, *123*(6), 5190–5208. https://doi.org/https://doi.org/10.1029/2017JB015121

Jochum, K. P., Stoll, B., Herwig, K., Willbold, M., Hofmann, A. W., Amini, M., … Woodhead, J. D. (2006). MPI-DING reference glasses for in situ microanalysis: New reference values for element concentrations and isotope ratios. *Geochemistry*, *Geophysics*, *Geosystems*, *7*(2), Q02008. https://doi.org/https://doi.org/10.1029/2005GC001060

Karson, J. A. (2017). The Iceland Plate Boundary Zone: Propagating Rifts, Migrating Transforms, and Rift-Parallel Strike-Slip Faults. *Geochemistry*, *Geophysics*, *Geosystems*, *18*(11), 4043–4054. https://doi.org/https://doi.org/10.1002/2017GC007045

Kelemen, P. B., Braun, M., Hirth, G. (2000). Spatial distribution of melt conduits in the mentle beneath spreading ridges: Observations from the Ingalls and Oman ophiolites. *Geochemistry, Geophysics, Geosystems,* 1(7), 1005. https://doi.org/10.1029/1999GC000012

Kelemen, P. B., Dick, H. J. B. (1995). Focused melt flow and localized deformation in the upper mantle: Juxtaposition of replacive dunite and ductile shear zones in the Josephine peridotite, SW Oregon. *Journal of Geophysical Research*, 100, 423-438. https://doi.org/10.1029/94JB02063

Kelemen, P. B., Shimizu, N., Salters, V. J. M. (1995). Extraction of mid-ocean-ridge basalt from upwelling mantle by focussed flow of melt in dunite channels. *Nature*, 375, 747-753. https://doi.org/10.1038/375747a0

Kent, A. J. R. (2008). Melt Inclusions in Basaltic and Related Volcanic Rocks. *Reviews in Mineralogy and Geochemistry*, *69*(1), 273–331. https://doi.org/10.2138/rmg.2008.69.8

Kerr, A. C., Saunders, A. D., Tarney, J., Berry, N. H., & Hards, V. L. (1995). Depleted mantle-plume geochemical signatures: no paradox for plume theories. *Geology*, *23*(9), 843–846. https://doi.org/10.1130/0091-7613(1995)023<0843:DMPGSN>2.3.CO;2

Kogiso, T., Hirose, K., & Takahashi, E. (1998). Melting experiments on homogeneous mixtures of peridotite and basalt: Application to the genesis of ocean island basalts. *Earth and Planetary Science Letters*, *162*(1–4), 45–61. https://doi.org/10.1016/S0012-821X(98)00156-3

Kokfelt, T. F., Hoernle, K., Hauff, F., Fiebig, J., Werner, R., & Garbe-Schönberg, D. (2006). Combined trace element and Pb-Nd-Sr-O isotope evidence for recycled oceanic crust (upper and lower) in the Iceland mantle plume. *Journal of Petrology*, *47*(9), 1705–1749. https://doi.org/10.1093/petrology/egl025

Lambart, S. (2017). No direct contribution of recycled crust in Icelandic basalts. *Geochemical Perspectives Letters*, *4*, 7–12. https://doi.org/http://dx.doi.org/10.7185/geochemlet.1728

Lawver, L. A., & Müller, R. D. (1994). Iceland hotspot track. *Geology*, *22*(4), 311–314. https://doi.org/10.1130/0091-7613(1994)022%3C0311:IHT%3E2.3.CO;2

Liang, Y., Schiemenz, A., Hesse, M. A., Paramentier, E. M., Hesthaven, J. A. (2010). High-porosity channels for melt migration in the mantle: Top is the dunite and bottom is the harzburgite and lherzolite. *Geophysical Research Letters*, 37, L15306. https://doi.org/10.1029/2010GL044162

Liang, Y., Schiemenz, A., Hesse, M. A., Paramentier, E. M. (2011). Waves, channels and the preservation of chemical heterogeneities during melt migration into the mantle. *Geophysical Research Letters*, 38, L20308. https://doi.org/10.1029/2011GL049034

Manning, C. J., & Thirlwall, M. F. (2014). Isotopic evidence for interaction between Öræfajökull mantle and the Eastern Rift Zone, Iceland. *Contributions to Mineralogy and Petrology*, *167*(1), 959. https://doi.org/10.1007/s00410-013-0959-1

Marschall, H. R., Wanless, V. D., Shimizu, N., Pogge von Strandmann, P. A. E., Elliott, T., &

Monteleone, B. D. (2017). The boron and lithium isotopic composition of mid-ocean ridge basalts and the mantle. *Geochimica et Cosmochimica Acta*, *207*, 102–138. https://doi.org/https://doi.org/10.1016/j.gca.2017.03.028

Matthews, S., Shorttle, O., & Maclennan, J. (2016). The temperature of the Icelandic mantle from olivine-spinel aluminum exchange thermometry. *Geochemistry, Geophysics, Geosystems, 17(11),* 4725-4752. https://doi.org/10.1002/2016GC006497

Matthews, S., Shorttle, O., Maclennan, J., & Rudge, J. F. (2021). The global melt inclusion C/Ba array: Mantle variability, melting process, or degassing? *Geochimica et Cosmochimica Acta*, *293*, 525–543. https://doi.org/10.1016/j.gca.2020.09.030

McKenzie, D., & O'nions, R. K. (1991). Partial melt distributions from inversion of rare earth element concentrations. *Journal of Petrology*, *32(5),* 1021-1091, https://doi.org/10.1093/petrology/32.5.1021

McKenzie, D., Stracke, A., Blichert-Toft, J., Albarède, F., Grönvold, K. & O'Nions, R. K. (2004). Source enrichment processes responsible for isotopic anomalies in oceanic island basalts. *Geochimica et Cosmochimica Acta, 68*, 2699–2724. http://doi.org/10.1016/j.gca.2003.10.029

Meyer, P. S., Sigurdsson, H., & Schilling, J. G. (1985). Petrological and geochemical variations along Iceland's neovolcanic zones. *Journal of Geophysical Research*, *90(B12*), 10043-10072 https://doi.org/10.1029/jb090ib12p10043

Miller, W. G. R., Maclennan, J., Shorttle, O., Gaetani, G. A., Le Roux, V., & Klein, F. (2019). Estimating the carbon content of the deep mantle with Icelandic melt inclusions. *Earth and Planetary Science Letters*, *523*, 115699 https://doi.org/10.1016/j.epsl.2019.07.002

Mukhopadhyay, S. (2012). Early differentiation and volatile accretion recorded in deep-mantle neon and xenon. *Nature*, *486*, 101–104. https://doi.org/10.1038/nature11141

Neave, D. A., Passmore, E., Maclennan, J., Fitton, G., & Thordarson, T. (2013). Crystal–Melt Relationships and the Record of Deep Mixing and Crystallization in the ad 1783 Laki Eruption, Iceland. *Journal of Petrology*, *54*(8), 1661–1690. https://doi.org/10.1093/petrology/egt027

Neave, D. A., Maclennan, J., Edmonds, M., & Thordarson, T. (2014). Melt mixing causes negative correlation of trace element enrichment and CO2 content prior to an Icelandic eruption. *Earth and Planetary Science Letters*, *400*, 272–283. https://doi.org/10.1016/j.epsl.2014.05.050

Neave, D. A., Shorttle, O., Oeser, M., Weyer, S., & Kobayashi, K. (2018). Mantle-derived trace element variability in olivines and their melt inclusions. *Earth and Planetary Science Letters*, *483*, 90–104. https://doi.org/10.1016/j.epsl.2017.12.014

Neave, D.A., Namur, O., Shorttle, O., Holtz, F. (2019). Magamatic evolution biases basaltic rock records towards melts from recycled sources. *Earth and Planetary Science Letters*, *520*, 199-211. https://doi.org/10.1016/j.epsl.2019.06.003

Nikogosian, I. K., & Sobolev, A. V. (1997). Ion-microprobe analysis of melt inclusions in olivine: experience in estimating the olivine-melt partition coefficients of trace elements. *Geochemistry International*, *35*, 119–126.

O'Neill, H. S. C., & Jenner, F. E. (2012). The global pattern of trace-element distributions in ocean floor basalts. *Nature*, *491*, 698-704. https://doi.org/10.1038/nature11678

Peate, D. W., Breddam, K., Baker, J. A., Kurz, M. D., Barker, A. K., Prestvik, T., Grassineau, N., Skovgaard, A. C. (2010). Compositional characteristics and spatial distribution of enriched Icelandic mantle components. *Journal of Petrology*, *51*(7), 1447–1475. https://doi.org/10.1093/petrology/egq025

Pertermann, M., & Hirschmann, M. M. (2003). Partial melting experiments on a MORB-like pyroxenite between 2 and 3 Gpa: Constraints on the presence of pyroxenite in basalt source regions from solidus location and melting rate. *Journal of Geophysical Research: Solid Earth*, *108*(B2). https://doi.org/https://doi.org/10.1029/2000JB000118

Prestvik, T., Goldberg, S., Karlsson, H., & Grönvold, K. (2001). Anomalous strontium and lead isotope signatures in the off-rift Öræfajökull central volcano in south-east Iceland: Evidence for enriched endmember(s) of the Iceland mantle plume? *Earth and Planetary Science Letters*, *190*(3–4), 211–220. https://doi.org/10.1016/S0012-821X(01)00390-9

Putirka, K. D. (2008). Thermometers and Barometers for Volcanic Systems. *Reviews in Mineralogy and Geochemistry*, *69*(1), 61–120. https://doi.org/10.2138/rmg.2008.69.3

Rasmussen, M. B., Halldórsson, S. A., Gibson, S. A., & Guðfinnsson, G. H. (2020). Olivine chemistry reveals compositional source heterogeneities within a tilted mantle plume beneath Iceland. *Earth and Planetary Science Letters*, *531*, 116008. https://doi.org/10.1016/j.epsl.2019.116008

Roberts, M. J., Gudmundsson, S. (2015). Oræfajökull Volcano: Geology and historical floods. In Pagneux, E., Gudmundsson, M. T., Karlsdóttir, S., Roberts, M. J. (Eds). *Volcanogenic floods in Iceland: An assessment of hazards and risks at Oræfajökull and on the Markarfljót outwash plain* (pp. 17–44). Reykjavík: IMO, IES-UI, NCIP-DCPEM

Roeder, P. L., & Emslie, R. F. (1970). Olivine-liquid equilibrium. *Contributions to Mineralogy and Petrology*. https://doi.org/10.1007/BF00371276

Rudge, J. F., Maclennan, J., & Stracke, A. (2013). The geochemical consequences of mixing melts from a heterogeneous mantle. *Geochimica et Cosmochimica Acta*, *114*, 112–143. https://doi.org/10.1016/j.gca.2013.03.042

Salters, V. J. M., & Stracke, A. (2004). Composition of the depleted mantle. *Geochemistry, Geophysics, Geosystems*, *5*(5). https://doi.org/https://doi.org/10.1029/2003GC000597

Schipper, C. I., Le Voyer, M., Moussallam, Y., White, J. D. L., Thordarson, T., Kimura, J.-I., & Chang, Q. (2016). Degassing and magma mixing during the eruption of Surtsey Volcano

(Iceland, 1963–1967): the signatures of a dynamic and discrete rift propagation event. *Bulletin of Volcanology*, *78*(4), 33. https://doi.org/10.1007/s00445-016-1025-4

Schnetzler, C. C., & Philpotts, J. A. (1970). Partition coefficients of rare-earth elements between igneous matrix material and rock-forming mineral phenocrysts-II. *Geochimica et Cosmochimica Acta*. https://doi.org/10.1016/0016-7037(70)90110-9

Shishkina, T. A., Botcharnikov, R. E., Holtz, F., Almeev, R. R., & Portnyagin, M. V. (2010). Solubility of H2O- and CO2-bearing fluids in tholeiitic basalts at pressures up to 500Mpa. *Chemical Geology*, *277*(1), 115–125. https://doi.org/https://doi.org/10.1016/j.chemgeo.2010.07.014

Shorttle, O., & Maclennan, J. (2011). Compositional trends of Icelandic basalts: Implications for short-length scale lithological heterogeneity in mantle plumes. *Geochemistry, Geophysics, Geosystems*, *12*(11). https://doi.org/10.1029/2011GC003748

Shorttle, O., Maclennan, J., & Lambart, S. (2014). Quantifying lithological variability in the mantle. *Earth and Planetary Science Letters*, *395*, 24–40. https://doi.org/10.1016/j.epsl.2014.03.040

Shorttle, O., Maclennan, J., & Piotrowski, A. M. (2013). Geochemical provincialism in the Iceland plume. *Geochimica et Cosmochimica Acta*, *122*, 363–397. https://doi.org/10.1016/j.gca.2013.08.032

Shorttle, O., Matthews, S., & Maclennan, J. (2020). Finding harzburgite in the mantle. A comment on Brown et al. (2020): “Markov chain Monte Carlo inversion of mantle temperature and source composition, with application to Reykjanes Peninsula, Iceland” [Earth Planet. Sci. Lett. 532 (2020) 116007]. *Earth and Planetary Science Letters*, *548*, 116503. https://doi.org/https://doi.org/10.1016/j.epsl.2020.116503

Spice, H. E., Fitton, J. G., & Kirstein, L. A. (2016). Temperature fluctuation of the Iceland mantle plume through time. *Geochemistry, Geophysics, Geosystems*. https://doi.org/10.1002/2015GC006059

Spiegelman, M., Kelemen, P. B. (2003). Extreme chemical variability as a consequence of channelized melt transport. *Geochemistry, Geophysics, Geosystems.* 4(7). https://doi.org/10.1029/2002GC000336

Spiegelman, M., Kelemen, P. B., Aharonov, E. (2001). Causes and consequences of flow organization during mantle transport: The Reaction Infiltration Instability in compactible media. *Journal of Geophysical*, 106, 2061-2077. https://doi.org/10.1029/2000JB900240

Staples, R. K., White, R. S., Brandsdóttir, B., Menke, W., Maguire, P. K. H., & McBride, J. H. (1997). Färoe-Iceland Ridge Experiment 1. Crustal structure of northeastern Iceland. *Journal of Geophysical Research: Solid Earth*, *102*(B4), 7849–7866. https://doi.org/10.1029/96JB03911

Suhr, G. (1999). Melt migration under Oceanic Ridges: Inferences from Reactive Transport Modelling of Upper Mantle Hosted Dunites. *Journal of Petrology*, 40(4), 575-599. https://doi.org/10.1093/petroj/40.4.575

Sun, S. -s., & McDonough, W. F. (1989). Chemical and isotopic systematics of oceanic basalts: implications for mantle composition and processes. *Geological Society, London, Special Publications*, *42*(1), 313 LP – 345. https://doi.org/10.1144/GSL.SP.1989.042.01.19

Thirlwall, M. F., Gee, M. A. M., Taylor, R. N., & Murton, B. J. (2004). Mantle components in Iceland and adjacent ridges investigated using double-spike Pb isotope ratios. *Geochimica et Cosmochimica Acta*. https://doi.org/10.1016/S0016-7037(03)00424-1

Weatherly, S. M., Katz, R. F. (2012). Melting and channelized magmatic flow in chemically heterogeneous, upwelling mantle. *Geochemistry, Geophysics, Geosystems*, *13*, Q0AC18. http://dx.doi.org/10.1029/2011GC003989

Wolfe, Cecily, J., Bjarnason, I. T., VanDecar, J. C., & Solomon, S. C. (1997). Seismic structure of the Iceland mantle plume. *Nature*, *385*, 245–247. https://doi.org/10.1038/385245a0

Wilson, S. A. (1997). *The collection, preparation and testing of USGS reference material BCR-2, Columbia River, Basalt*, U.S. Geological Survey Open-File Report 98-00X

Yaxley, G. M., Green, D. H. (1998). Reactions between eclogite and peridotite: mantle refertilisation by subduction of oceanic crust. *Swiss Journal of Geosciences Supplement*, 78, 243-255